Data in Brief 35 (2021) 106846

Contents lists available at ScienceDirect

Data in Brief

journal homepage: www.elsevier.com/locate/dib

Data Article

Petrological, geochemical (major, trace, and rare earth elements), and U–Pb zircon data of the Tamatán Group, NE Mexico

Juan Moisés Casas-Peña[a], Juan Alonso Ramírez-Fernández[b], Fernando Velasco-Tapia[b], Eduardo Alejandro Alemán-Gallardo[a], Carita Augustsson[c], Bodo Weber[d], Dirk Frei[e], Uwe Jenchen[b,*]

[a] *Programa de Posgrado de la Facultad de Ciencias de la Tierra, Universidad Autónoma de Nuevo León, Carr. Cerro Prieto Km 8, Ex. Hacienda de Guadalupe, Linares, NL 67700, Mexico*
[b] *Universidad Autónoma de Nuevo León (UANL), Facultad de Ciencias de la Tierra, Carr. Cerro Prieto Km 8, Ex. Hacienda de Guadalupe, Linares, NL 67700, Mexico*
[c] *Department of Energy Resources, Universitetet i Stavanger, Faculty of Science and Technology, 4036 Stavanger, Norway*
[d] *Departamento de Geologiá, Centro de Investigación Científica y de Educación Superior de Ensenada (CICESE), Ensenada, Mexico*
[e] *Department of Earth Sciences, University of the Western Cape, Cape Town, South Africa*

ARTICLE INFO

Article history:
Received 7 January 2021
Revised 23 January 2021
Accepted 2 February 2021
Available online 17 February 2021

Keywords:
Gondwana
Huizachal peregrina anticlinorium
Paleozoic
Sedimentary petrology
Geochemistry
U-Pb geochronology

ABSTRACT

From samples of the Paleozoic Tamatán Group (Huizachal–Peregrina Anticlinorium, Tamaulipas, Mexico), petrographic (qualitative and modal) and geochemical analyses (major, trace, and rare earth elements) were conducted. The first U–Pb geochronological data on detrital zircons of the Tamatán Group were generated using four samples. The data presented here contains a broad overview of photomicrography, recalculated modal point-count data, raw geochemical data, and simple statistics of selected geochemical parameters. The data presented in this article are interpreted and discussed in the research article titled "Provenance and tectonic setting of the Tamatán Paleozoic sequence, NE Mexico: Implications for the closure of the Rheic Ocean at the northwestern part of Gondwana" [1].

DOI of original article: 10.1016/j.gr.2020.12.012
* Corresponding author.
E-mail address: uwe.jenchen@uanl.edu.mx (U. Jenchen).
Social media: (J.M. Casas-Peña), (J.A. Ramírez-Fernández), (E.A. Alemán-Gallardo), (U. Jenchen)

https://doi.org/10.1016/j.dib.2021.106846

Specifications Table

Subject	Earth Sciences
Specific subject area	Petrology, geochemistry, U–Pb geochronology
Type of data	Microscopy and CL images, tables, figures, and graphs
How data was acquired	Seventy-three samples were pulverized and analyzed using ICP-ES (oxides, Ba, Ni, and Sc) and ICP-MS (trace and rare earth elements) at ACME Laboratories, Vancouver, Canada. The U–Pb analysis followed standard procedures and was carried out at the Geology Department at Centro de Investigación Científica y de Educación Superior de Ensenada Baja California. U–Pb data of four samples were analyzed in detrital zircon grains using laser ablation multicollector inductively coupled plasma mass spectrometry at the Central Analytical Facilities, Stellenbosch University, South Africa.
Data format	Raw (photos, geochemical, and U–PB data), analyzed, processed, and filtered data.
Parameters for data collection	Representative samples for each geological unit were collected in the Peregrina and Caballeros canyons. Thin sections were prepared, point-counted, and photographed.
Description of data collection	Petrological, geochemical, and U–Th–Pb analysis of the sedimentary rocks of the Tamatán Group.
Data source location	Huizachal–Peregrina Anticlinorium, Tamaulipas, Mexico. Caballeros Canyon (23°47.7′–23°49.2′N, and 99°16.8′–99°18′W) Peregrina Canyon (23°46.2′–23°47 °.4 N and 99°14.7–99°16.5W
Data accessibility	Data available within this article and in https://data.mendeley.com/datasets/wbzzy6hcgj/1.
Related research article	Casas-Peña, M., Ramírez-Fernández, J.A., Velasco-Tapia, F., Alemán-Gallardo, E.A., Augustsson, C., Weber, B., Frei, D. & Jenchen, U. (en prep): Provenance and tectonic setting of the Paleozoic Tamatán Group, NE Mexico: Implications for the closure of the Rheic Ocean – Gondwana Research 91 (2021) xxx. – [doi: https://doi.org/10.1016/j.gr.2020.12.012] [1]

Value of the Data

- First comprehensive data set of selected data from the Paleozoic Tamatán Group, NE México, including petrográphical, geochemical, and Uran/Lead data of all described formations.
- Important information to complete an integrated geological model for the Northwestern Margin of Gondwana and adjacent areas.
- Raw-, and processed data to work with studies of tectonic activity, weathering, and provenance of the Paleozoic sequences of NE Mexico and sedimentary rocks of comparable tectonic settings. This set also includes data which are not used in the related research article to be useful for further investigations.

1. This Article

This article provides selected data from 105 samples (for the complete data set, please consult [2]). From 70 samples, photomicrographs were taken and point-counted and modal analyses on recalculated petrographic parameters were provided. Geochemical analyses (major, trace, and rare earth elements [REE]) of 73 samples were conducted. Four samples for U–Pb geochronological zircon analyses were made. The sample location is given with the geographical and UTM coordinates of each sample. Each sample is located on a geological map. The petrographic and geochemical data are presented as raw data and displayed as a simple statistic of the selected

petrography and geochemical parameters, respectively. Additionally, outcrop photographs are provided.

- Fig. 1: Geological maps of the sampling area to locate the detailed sample collection areas of the different geological units.
- Fig. 2: Location of the collected samples in a stratigraphic column to provide the stratigraphic position of each of the samples.
- Figs. 3–7: Photographs documenting the outcrops of the Cañón de Caballeros Formation (Fig. 3), the Vicente Guerrero Formation (Fig. 4), the Del Monte Formation (Fig. 5), and the Guacamaya Formation (Figs. 6 and 7).
- Table 1: Description of selected samples and its geographical location with coordinates and UTM data. Complete data see Table 1 in [2].
- Table 2: Detailed list of the parameters and characteristics used for statistical point counting of the thin sections.
- Table 3: Raw data of selected point counted thin sections (this table shows the values in counted grains). Complete table see Table 3 in [2].
- Table 4: Recalculated data of selected point counted parameters in thin sections (this table shows the percentage of the total value). Complete data see Table 4 in [2].
- Table 5: Recalculated modal and ternary index data of selected samples. Complete data see Table 5 in [2]. The data for each ternary diagram has to be recalculated to achieve 100% in total. Qt–F–L+Ch after [3]; Qt–F–L tafter [4] and [5]; Qm–F–Lt after [4]; Qm–K–P after [6]; Lm–Lv–Ls and Qp–Lv–Ls after [3] and [5]. Included are the recalculated statistical parameters of the arithmetical mean and the 95% and 99% statistical confidence limits after Student [7].
- Figs. 8–11: Detailed geological map documenting the sample locations of the Cañón de Caballeros Formation (Fig. 8), the Vicente Guerrero Formation (Fig. 9), the Del Monte Formation (Fig. 10), and the Guacamaya Formation (Fig. 11).
- Tables 6–9: Photomicrographs of selected sections from the Cañón de Caballeros Formation (Table 6), the Vicente Guerrero Formation (Table 7), the Del Monte Formation (Table 8), and the Guacamaya Formation (Table 9). On the left side a standard magnification with parallel and crossed nicols and on the right side detail enlargements from the same perspective, also with parallel and crossed nicols. Complete data see Tables 6–9 in [2].
- Fig. 12: Recalculated petrographic point counting data, mean-, and confidential limits plotted, separated for each stratigraphic unit, into the Q–F–L diagram after [3].
- The Figs. 12–15 contain recalculated petrographic point counting data, mean-, and confidential limits plotted, separated for each stratigraphic unit, into the Q–F–L diagram after [8] (Fig. 12), Qm–P–K diagram after [6] (Fig. 13), the Q–F–L diagram after [4] (Fig. 14), and the Qm–F–Lt diagram after [9] (Fig. 15).
- The Tables 10 and 11 contain geochemical raw data and selected (recalculated) geochemical parameters of selected samples from the Cañon de Caballeros Formation and the Vicente Guerrero Formation (Table 10), and, from the Del Monte Formation and the Guacamaya Formation (Table 11). Note: Oxides and LOI in%, other elements in ppm. Abbreviations: n.d.: not detected; $CaCO^{*}$ = maximum CaO in Carbonates recalculated from CO_2; Chem.Lit: Chemical lithology [10]; CaO++: CaO enriched samples; Psam.: Psammite classified samples; Rest++: enriched in Si_{O2} and $Al2O_3$; Rest−: impoverished in SiO_2 and Al_2O_3; $Eu/Eu^{*}=Eu_N/(Sm_N x Gd_N)0.5$; REE= La_N/Lu_N; LREE=La_N/Sm_N; HREE=Gd_N/Lu_N; Σ-REE= Total REE (in ppm); Samples are not LOI-free recalculated. Complete data see Tables 10–13 in [2].
- Table 12 (Table 14 in [2]): Simple statistics of the selected geochemical parameters which are used in the discrimination diagrams. Included are the recalculated statistical parameters of the arithmetical mean and the 95% and 99% statistical confidence limits after Student [7].
- Table 13 (Table 15 in [2]): Simple statistics of the rare earth elements (REE). Included are the recalculated statistical parameters of the arithmetical mean and the 95% and 99% statistical confidence limits after Student [7].
- The Figs. 16–24 contain data from sedimentary whole rock geochemical analysis (mean-, and confidential limits are recalculated) plotted, separated for each stratigraphic unit, plotted into

the SiO_2–Al_2O_3 diagram after [10] (Fig. 16), the K_2O–Na_2O diagram after [11]. (Fig. 17), the Na_2O+CaO–Al_2O_3–K_2O diagram after [12,13] modified by [10] (Fig. 18); the Zr/Sc–Th/Sc diagram after [14] (Fig. 19), the Th/Sc–Cr diagram after [10] (Fig. 20), the SiO_2/K_2O–Ti/Nb diagram after [10] (Fig. 21), the K_2O/Na_2O–SiO_2/Al_2O3 diagram after [10] (Fig. 22), the Th–Co–Zr/10 diagram after [15] (Fig. 23), and the REE-Spider diagram after [16] (Fig. 24).

- The Tables 14, 16, 18, and 20 of this paper contain LA-MC-ICPMS U-Th-Pb raw and processed data of selected detrital zircons from Cañón de Caballeros Formation (Table 14), Vicente Guerrero Formation (Table 16) Del Monte Formation (Table 18), and the Guacamaya Formation (Table 20). Complete data see Tables 16, 18, 20, and 22 in [2].
- The Figs. 25–28 show unfiltered CL images (raw images) of the collection of zircons from sample CC64–04 (Cañón de Caballeros Formation; Fig. 25), sample CC54–14 (Vicente Guerrero Formation; Fig. 26), sample C9207–07 (Del Monte Formation; Fig. 27), and sample CP197–03 (Guacamaya Formation; Fig. 28). See also Figs. 46–49 in [2].
- The Tables 15, 17,19, and 21 of this paper contain single grain CL-images of selected measured zircons of the Cañón de Caballeros Formation (Table 15), the Vicente Guerrero Formation (Table 17), the Del Monte Formation (Table 19), and the Guacamaya Formation (Table 21), amplified from the figures Figs. 25–28 (complete data see [2]). The images are arranged in descending order of the best ages. The colors of the boxes correspond to the colors of the International Chronostratigraphic Table of the respective System/Period (for Precambrian ages) or Series/Epoch (for Paleozoic ages). Complete data see Tables 17, 19, 21, and 23 in [2].
- Tables 24–39 in [2] show the single grain CL-images of selected measured zircon of the Siderian (Table 24), Statherian (Table 25), Calymmian (Table 26), Ectasian (Table 27), Stenian (Table 28), Tonian (Table 29), Cryogenian (Table 30), Ediacaran (Table 31), Cambrian (Table 32), Ordovician (Table 33), Silurian (Table 34), Devonian (Table 35), Mississippian (Table 36), Pennsylvanian (Table 37), Permian (Table 38), and Triassic (Table 39) ages, amplified from the Figs. 46–49. The images are arranged in descending order of the best ages. The colors of the boxes correspond to the color of the respective stratigraphic unit as used in the whole text (blue: Cañón de Caballeros Fm.; green: Vicente Guerro Fm.; red: Del Monte Fm.; and yellow: Guacamaya Fm.).

2. Supplemantary Data Set

The supplementary data set provides the complete data from 105 samples. From 70 samples, photomicrographs were taken and point-counted and modal analyses on recalculated petrographic parameters were provided. Four samples for U–Pb geochronological zircon analyses were made. The sample location is given with the geographical and UTM coordinates of each sample. Each sample is located on a geological map.Outcrop photographs are provided. Geochemical analyses (major, trace, and rare earth elements [REE]) of 73 samples were conducted. The petrographic and geochemical data are presented as raw data and displayed as a simple statistic of the selected petrography and geochemical parameters, respectively. Petrographical and geochemical compositional data and its arithmetic mean and confidence limits (95% and 99%, respectively) are plotted into the most common diagrams offered by several authors. The supplementary data set contains single zircon CL-images and best ages of each zircon ($<$ 400 grains) of the Cañón de Caballeros Formation, the Vicente Guerrero Formation, the Del Monte Formation, and the Guacamaya Formation. Also single grain CL-images of each measured zircon of the Siderian, Statherian, Calymmian, Ectasian, Stenian, Tonian, Cryogenian, Ediacaran, Cambrian, Ordovician, Silurian, Devonian, Mississippian, Pennsylvanian, Permian, and Triassicages, amplified from the Figs. 46–49. The images are arranged in descending order of the best ages.

3. Experimental Design, Materials and Methods

The cartographic basis for the fieldwork comprised topographical maps of the Instituto Nacional de Estadística y Geografía (INEGI) on a scale of 1:10,000 and is based on geological maps

proposed by Stewart et al. [17] and [18]. The outcrops (Fig. 1) and sample sites were located on the geological map. A detailed description of the sampling and sample processing is given in Table 1.

Thin sections, documented in Tables 6–9, are characterized and photographed using a Leica MC170HD polarization microscope and a HC FL PLAN 2.5×0.07 camera under parallel and crossed Nicols conditions. According to the Gazzi–Dickinson technique to minimize the effects of the size of the clasts, modal analyses were performed on 71 samples by counting 400–600 points. The modal composition and statistical parameters of the point counting were based on previous works [3,5,6,4,9,8]. The 95% and 99% confidence intervals for Student's *t*-test [7] were plotted in optically distinct shades (see Figs. 12–20; Tables 2–5).

The analyses were performed using inductively coupled plasma optical emission spectrometry for major elements and inductively coupled plasma mass spectrometry for trace elements at ACME Analytical Laboratories Ltd. in Vancouver, Canada. The analyses are provided in Table 9. For this data collection, the distributions of the elements in the random samples were described using the arithmetic mean and confidence limits (95% and 99%, respectively) supplied by Student's *t*-test ([7]).

Four samples underwent U–Pb geochronological analysis. A detailed description of the geochronological processing and analytic methods is given [1]. The raw and processed data of selected samples are listed in Tables 14, 16, 18, and 20. The four samples were processed following standard procedures at the geology department of Centro de Investigación Científica y de Educación Superior de Ensenada Baja California. U–Pb data were analyzed in zircon grains using laser ablation multicollector inductively coupled plasma mass spectrometry at the Central Analytical Facilities, Stellenbosch University, South Africa. All the geochronological data were plotted into the Wetherill Concordia and relative age probability diagram [19].

4. Figures and Tables

4.1. Geological setting and sampling

Figs. 1-7, Table 1.

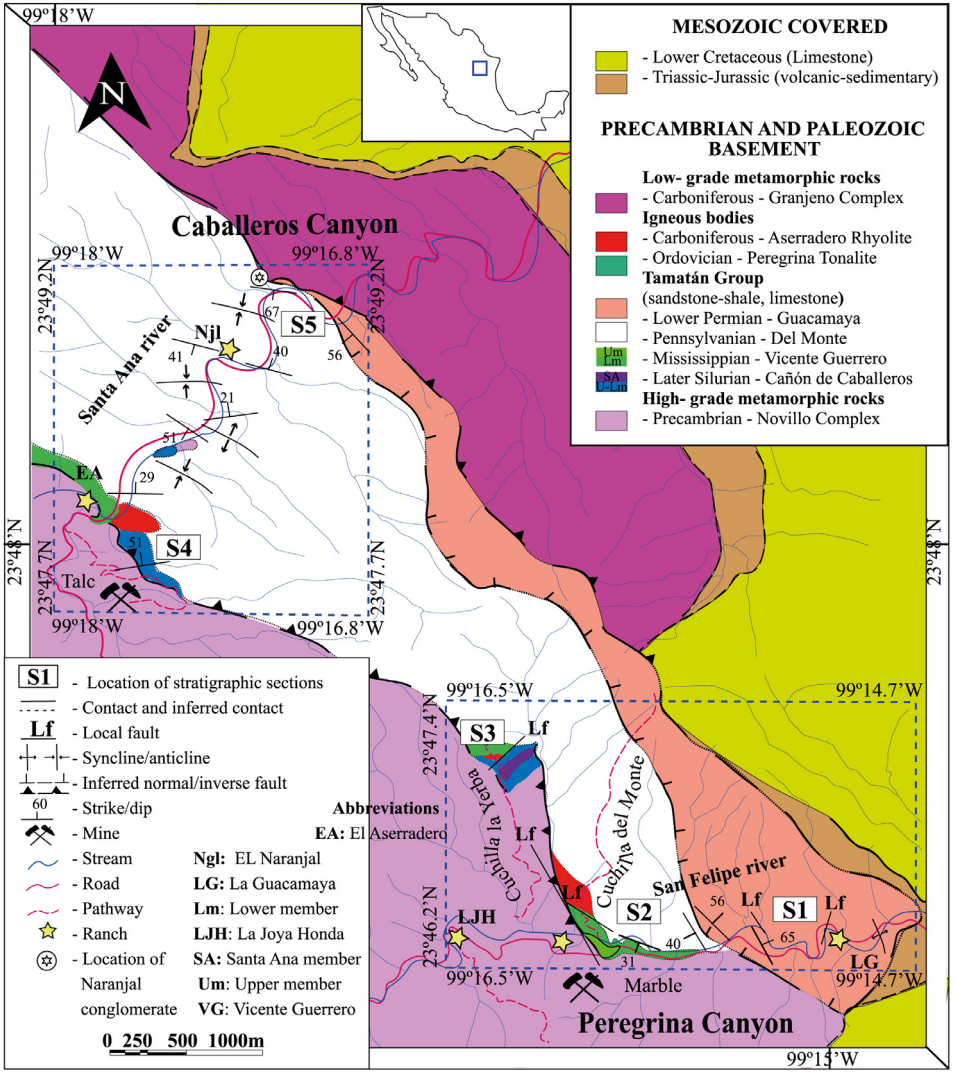

Fig. 1. Geological maps of the sampling area (modified from [17,18], and [20]).

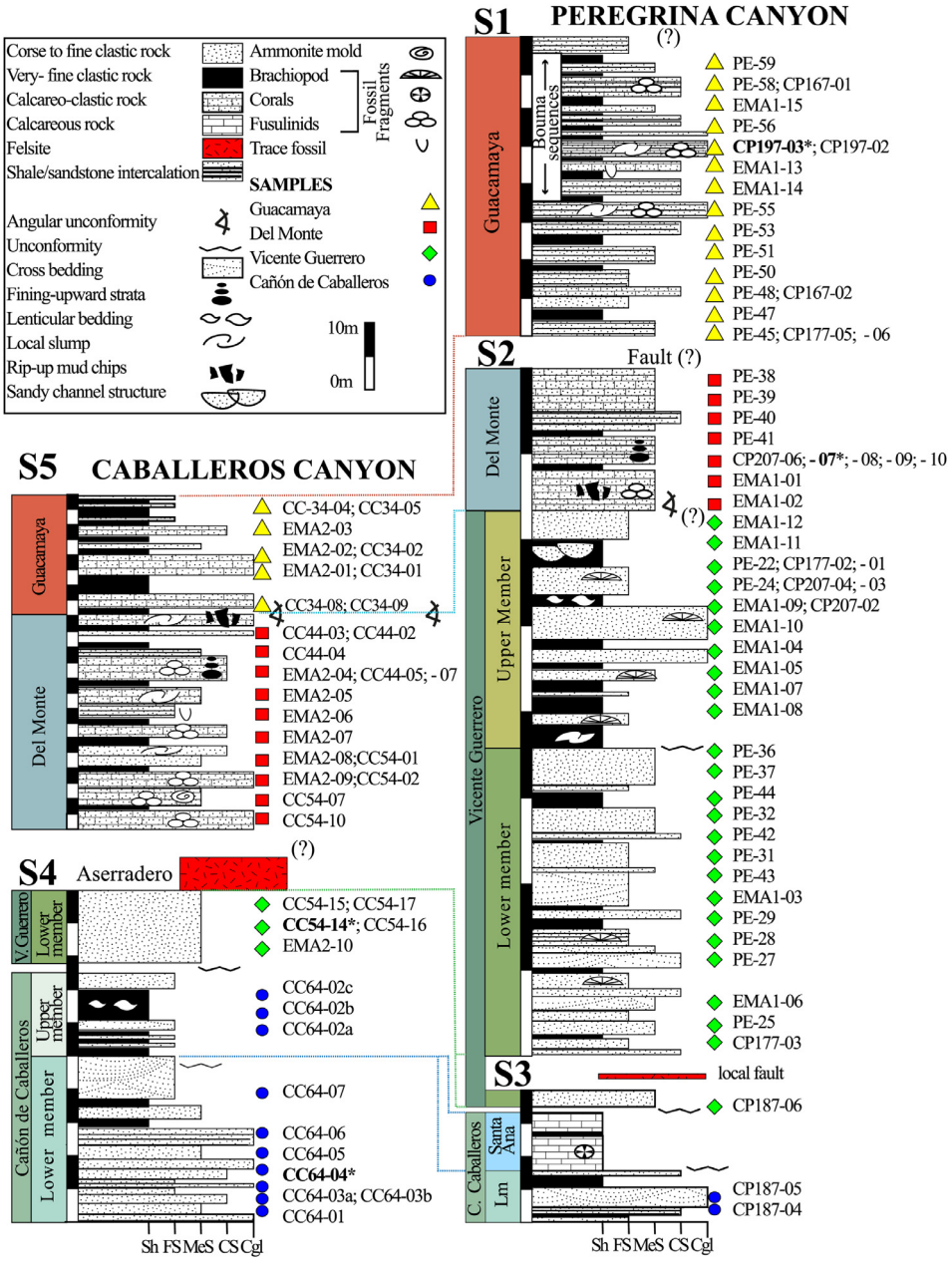

Fig. 2. Stratigraphic column and stratigraphic position of samples (modified after [1] and [17]).

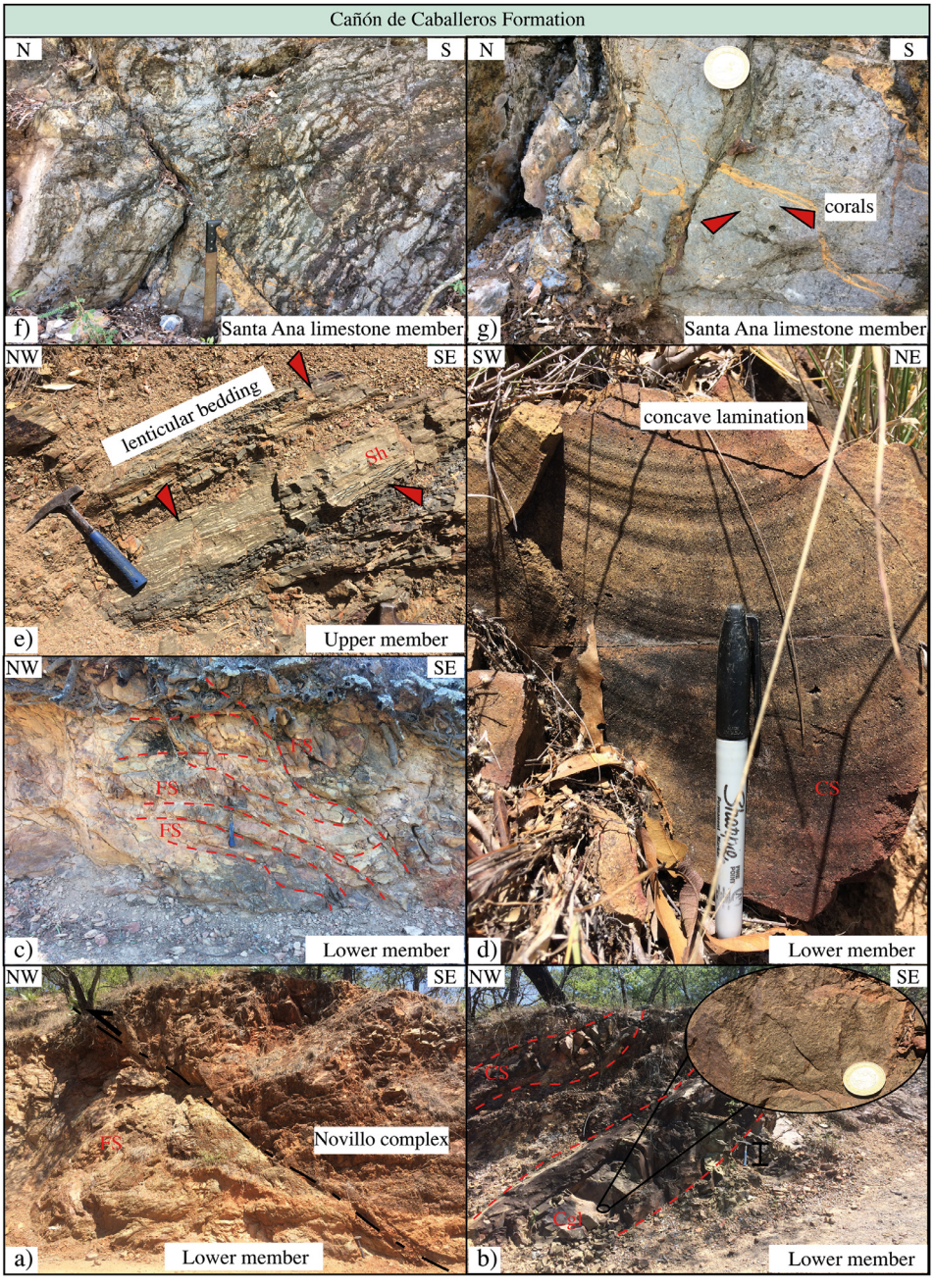

Fig. 3. Outcrop photographs from the Cañón de Caballeros Formation (Wenlock to Lower Devonian).

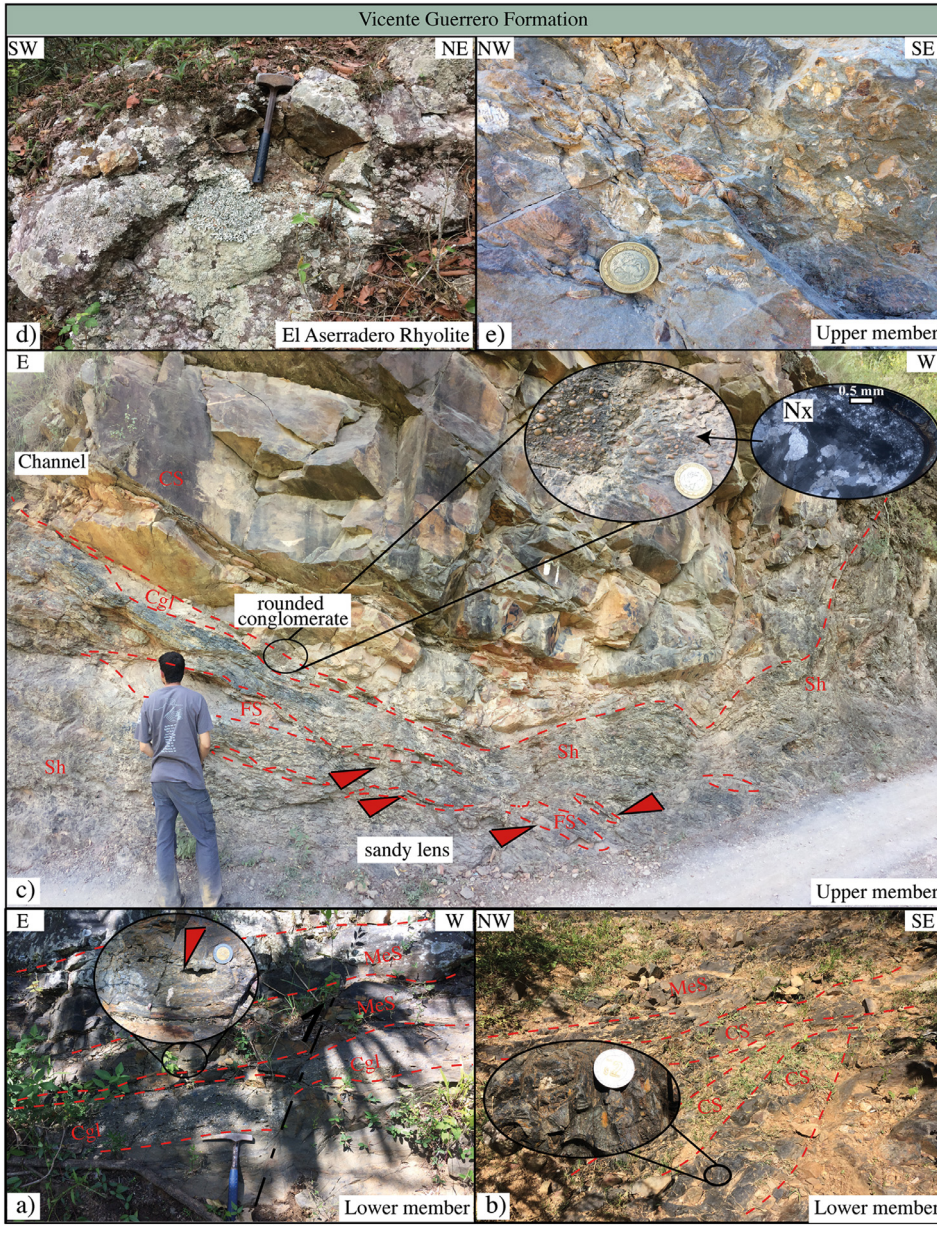

Fig. 4. Outcrop photographs from the Vicente Guerrero Formation (Lower Missisipian).

Fig. 5. Outcrop photographs from the Del Monte Formation (Lower Pennsylvanian).

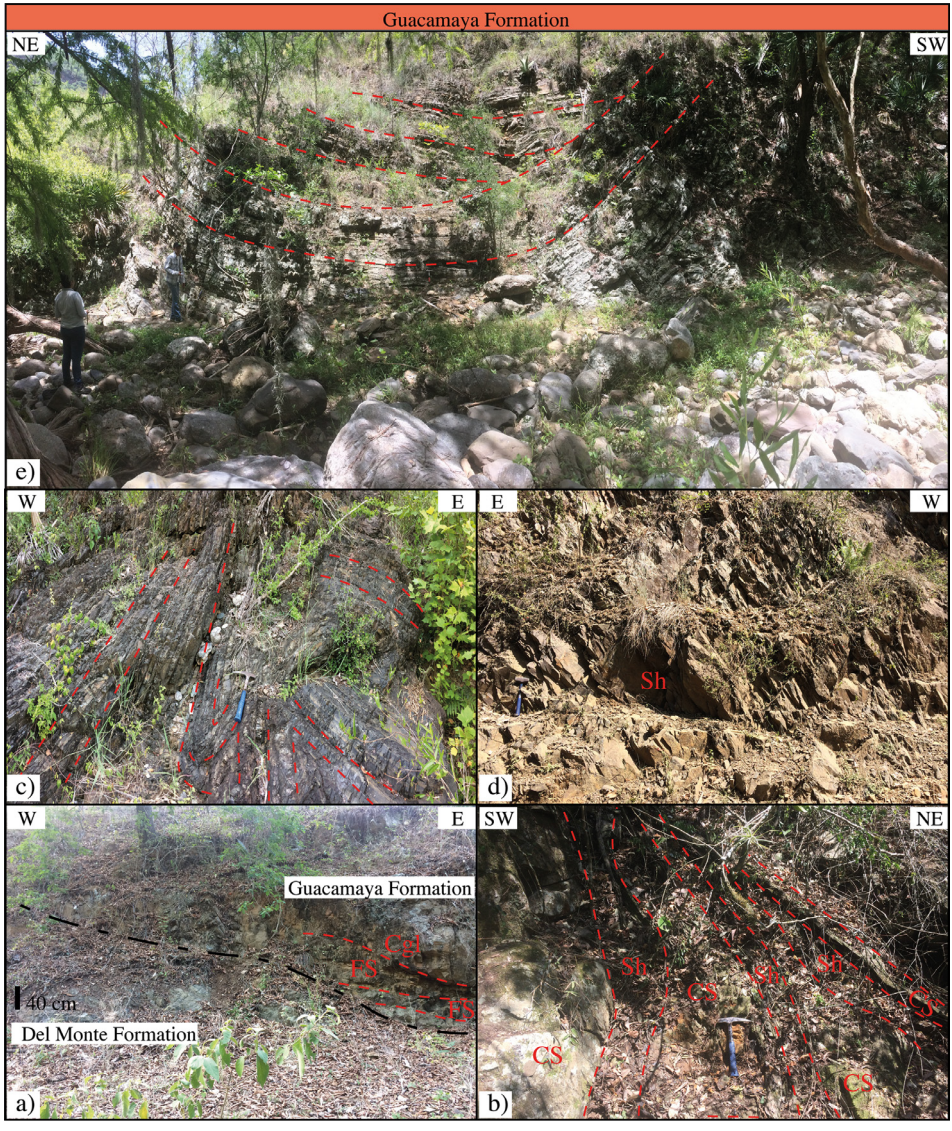

Fig. 6. Outcrop photographs of the Guacamaya Formation I (Lower Permian).

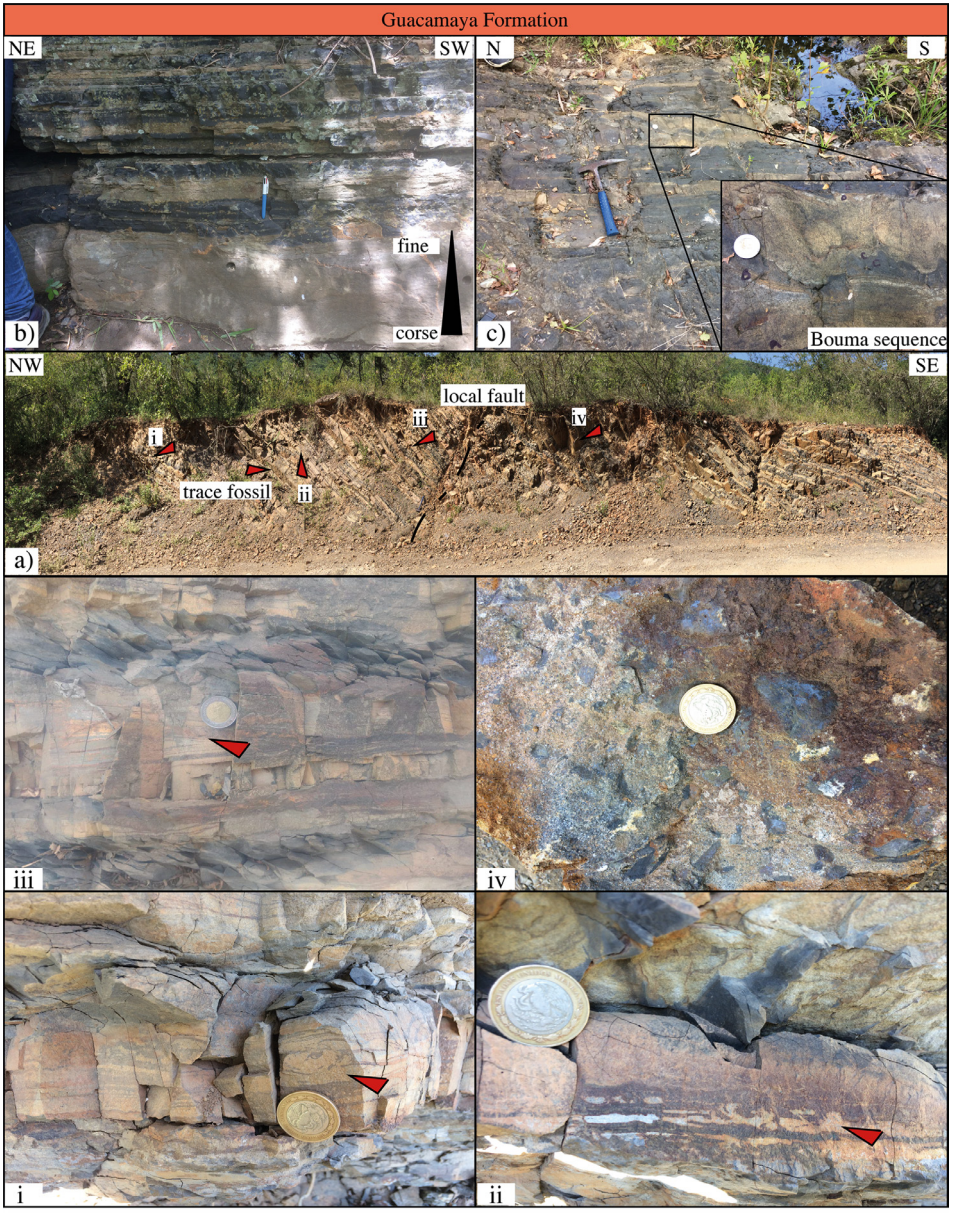

Fig. 7. Outcrop photographs from the Guacamaya Formation II (Lower Permian).

Table 1
Sample list and sample locations of selected samples (complete list see [2]).

Sample	Lithology	Canyon	Formation	UTM-E	UTM-N	Latitude (°N)	Longitude (°W)	Analytical Method		
								I	II	III
CC64–01	MeS	Caballeros	Cañón de Caballeros (Lm)	470,094	2,631,870	23°47′52.03″	99°17′36.85″	X	X	
CC64–02a	Sh	Caballeros	Cañón de Caballeros (Um)	470,153	2,631,822	23°47′50.47″	99°17′34.76″	X	X	
CC64–02b	Sh	Caballeros	Cañón de Caballeros (Um)	470,153	2,631,822	23°47′50.47″	99°17′34.76″	X	X	
CC64–03a	CS	Caballeros	Cañón de Caballeros (Lm)	470,276	2,631,703	23°47′46.61″	99°17′30.41″	X	X	
CC64–03b	CS	Caballeros	Cañón de Caballeros (Lm)	470,276	2,631,703	23°47′46.61″	99°17′30.41″	X	X	
CC64–04	CS	Caballeros	Cañón de Caballeros (Lm)	470,240	2,631,770	23°47′48.79″	99°17′31.69″	X	X	X
EMA1–04	Cgl	Peregrina	Vicente Guerrero (Um)	472,991	2,629,012	23°46′19.28″	99°15′54.29″	X	X	
EMA1–05	MeS	Peregrina	Vicente Guerrero (Um)	472,991	2,629,012	23°46′19.28″	99°15′54.29″	X	X	
EMA1–07	FS	Peregrina	Vicente Guerrero (Um)	472,889	2,629,075	23°46′21.32″	99°15′57.89″	X	X	
EMA2–10	MeS	Caballeros	Vicente Guerrero (Lm)	469,794	2,632,328	23°48′06.90″	99°17′47.49″	X	X	
CC54–14	MeS	Caballeros	Vicente Guerrero (Lm)	469,772	2,632,328	23°48′06.90″	99°17′47.49″	X	X	X
CC54–15	MeS	Caballeros	Vicente Guerrero (Lm)	469,772	2,632,328	23°48′06.90″	99°17′47.49″	X	X	
EMA1–01	MeS	Peregrina	Del Monte	473,140	2,629,008	23°46′19.16″	99°15′49.02″	X	X	
EMA1–02	MeS	Peregrina	Del Monte	473,072	2,629,012	23°46′19.29″	99°15′51.42″	X	X	
EMA2–06	FS	Caballeros	Del Monte	470,841	2,633,811	23°48′55.19″	99°17′10.59″	X	X	
EMA2–07	CS	Caballeros	Del Monte	470,841	2,633,811	23°48′55.19″	99°17′10.59″	X	X	
EMA2–09	Cgl	Caballeros	Del Monte	470,915	2,633,706	23°48′51.79″	99°17′07.97″	X	X	
CP207–07	MeS	Peregrina	Del Monte	473,181	2,629,063	23°46′20.95″	99°15′47.58″	X	X	X
EMA1–14	CS	Peregrina	Guacamaya	474,556	2,625,094	23°46′22.05″	99°14′59.00″	X	X	
EMA1–15	CS	Peregrina	Guacamaya	474,833	2,629,133	23°46′23.32″	99°14′49.21″	X	X	
EMA2–01	Cgl	Caballeros	Guacamaya	471,266	2,633,885	23°48′57.63″	23°16′55.58″	X	X	
EMA2–02	Cgl	Caballeros	Guacamaya	471,033	2,634,126	23°48′05.45″	99°17′03.83″	X	X	
CC34–08	Cgl	Caballeros	Guacamaya	471,235	2,633,893	23°48′57.88″	99°16′56.67″	X	X	
CP197–03	CS	Peregrina	Guacamaya	474,593	2,629,044	23°46′20.42″	99°14′57.69″	X	X	X

Abreviations: Sh= Shale, FS= Fine sandstone, MeS = Medium sandstone, CS= Coarse sandstone, Cgl = Conglomerate, Lm= Lower member, Um= Upper member. Methods of analyses: Pet.= Petrography, Gq = Geochemical and Gch = Geochronology.

4.2. Petrographical data

Tables 2-9, Figs. 8-15.

Table 2
Point counting parameters.

Counted	Grains/Fragments	Parameter	Calculation	Meaning
Qmr*	straight extinction monocrystalline quartz	Qm	Qm+Qmr+Cq	Monocrystalline quartz
Qmo*	undulatory monocrystalline quartz			
Qp2–3*	polycrystalline quartz with 2–3 units	Qp	Qp2–3+Qp< 3	Polycrystalline quartz
Qp>3*	polycrystalline quartz with >3 units			
Cq*	quartz with calcite and/or illite			
		Qt	Qm+Qp	Total stable quartz
Fk*	potassic feldspar without replacement	K	Fk+Fki+Frc	Potassic feldspar
Fki*	potassic feldspar with illite replacement			
Frc*	potassic feldspar with calcite replacement			
Pna*	sodic plagioclase without replacement	P	Pna+Pki+Prc	Plagioclase
Pki*	sodic plagioclase with illite/sericite replacement			
Prc*	sodic plagioclase with calcite replacement			
		F	K + P	Total feldspars
Lmf*	psammitic lithic	Lm	Lmf + Lmp	Metamorphic lithics
Lmp*	metapelitic lithic			
Lvf*	felsitic volcanic lithic,	Lv	Lvf+Lvt+Lvl+Lp	Igneous lithics
Lvt*	tobaceous volcanic lithic,			
Lvl*	lathwork volcanic lithic			
Lp*	plutonic lithic			
Lsa*	sandy sedimentary lithic	Ls	Lsa+Lslu+LsCe+LsCm+Fo+LsBi	Sedimentary lithics
Lslu*	shale/limolite sedimentary lithic			
LsCe**	sparitic sedimentary lithic			
LsCm**	micritic sedimentary lithic			
Fo**	microfossils			
LsBi***	bioclastic sedimentary lithic			
Ch	chert			
			Lt Lm+Lv+Ls	Total unstable lithic
M	mica (include biotite;Bt, muscovite; Ms and/or chlorite; Chl)			
Hm	heavy mineral (include: zircon; Zr and/or apatite; Ap)			

Abreviations: Cm = Calcitic cement / clay matrix, Sor. = sorted, P- M- W = poorly, moderate and well sorted, Ro. = roundness, Sub-a = sub-angular grains, Sub-r = sub-rounded grains, r = rounded grains, Ma = mature, SubMa = submature, InMa = innmature. * = Noncarbonate extrabasinal grains (NCE), ** = Carbonatic extrabasinal components (CE), *** = Carbonatic intrabasinal components (CI). The mainly parameters are in bold.

Table 3
Point-counting data.

Sample	Texture				Framework																				Frame-work total
	Granulometry	Maturity	Disposition		NCE														NCE total	Other paritcular components					
			Ro.	Sor.	Qt	Qmo	Qmr	Qp2-3	Qp>3	Cq	K	P	Lm	Lv	Ls	Ch				CE	CI	M	IM	Cm	
Cañón de Caballeros Formation																									
CC-64-01 (Um)	Medium	InMa	r	P	117	29	32	18	14	24	51	12	15	60	4	17	276	0	0	46	5	119	446		
CC-64-02a(Um)	Fine	SubMa	Sub-a	P	88	12	70	2	4	0	42	5	5	8	5	9	162	5	0	59	0	206	427		
CC-64-02b(Um)	Fine	InMa	Sub-a	P	109	3	89	4	13	0	49	3	5	22	9	17	214	0	0	30	1	221	466		
CC-64-03a(Lm)	Coarse	Ma	Sub-r	W	209	34	85	25	65	0	57	9	26	89	27	15	432	7	0	36	11	50	529		
CC-64-03b(Lm)	Coarse	SubMa	Sub-r	M	152	23	52	43	34	0	40	4	5	66	38	49	354	8	0	24	0	95	473		
CC-64-04 (Lm)	Coarse	SubMa	Sub-a	M	207	44	70	28	50	15	40	15	16	80	29	20	407	17	0	24	10	87	528		
Vicente Guerrero Formation																									
EMA1-04 (Um)	Coarse	SubMa	Sub-a	M	169	5	106	35	23	0	121	4	10	42	12	25	383	2	0	90	13	155	641		
EMA1-05 (Lm)	Fine	InMa	Sub-a	M	212	56	111	37	8	0	84	16	10	7	86	14	429	21	3	65	2	8	124	613	
EMA1-07 (Um)	Fine	InMa	Sub-a	M	206	49	67	61	9	20	119	6	10	21	38	12	412	0	0	68	15	95	590		
EMA2-10 (Lm)	Medium	Ma	Sub-r	W	227	49	90	41	29	18	73	4	16	39	27	15	401	0	0	52	14	75	542		
CC-54-14 (Lm)	Medium	Ma	Sub-r	W	235	59	101	44	31	0	65	2	6	30	60	4	402	0	0	0	10	85	497		
CC-54-15 (Lm)	Medium	Ma	Sub-r	W	235	68	95	41	31	0	80	3	6	32	57	12	425	0	0	50	9	79	563		
Del Monte Formation																									
EMA1-01	Medium	InMa	a	P	159	49	54	14	23	12	104	74	17	64	39	17	467	9	7	44	0	100	611		
EMA1-02	Medium	InMa	Sub-r	M	149	48	62	9	15	15	110	85	12	71	66	10	503	40	0	64	6	127	700		
EMA2-06	Fine	SubMa	a	M	142	32	64	22	10	14	109	84	3	55	25	12	430	0	0	82	13	149	674		
EMA2-07	Coarse	SubMa	Sub-r	M	130	33	57	5	23	12	102	81	5	41	74	0	433	44	0	61	9	106	609		
EMA2-09	Coarse	SubMa	Sub-a	M	131	30	67	6	14	14	72	29	12	54	86	0	384	67	0	7	5	120	516		
CP-207-07	Coarse	SubMa	Sub-a	P	147	48	39	12	16	12	67	52	29	84	35	10	404	0	1	62	2	10	98	534	
Guacamaya Formation																									
EMA1-14	Coarse	SubMa	Sub-r	M	139	16	63	35	10	15	68	72	59	128	69	10	545	28	1	43	3	5	95	678	
EMA1-15	Coarse	SubMa	Sub-a	M	114	12	63	10	14	15	71	80	14	152	50	7	488	22	2	32	2	3	89	602	
EMA2-01	Corse	Ma	Sub-r	M	131	12	63	22	15	19	67	69	9	107	64	8	455	31	1	31	1	0	105	571	
EMA2-02	Coarse	Ma	Sub-r	M	124	24	71	8	11	10	58	80	14	131	28	5	440	0	0	7	3	68	518		
CC34-08	Coarse	InMa	Sub-r	P	119	18	47	11	16	27	88	87	27	32	13	27	393	0	0	7	2	98	500		
CP197-03	Coarse	Ma	Sub-r	M	105	23	47	13	15	7	46	48	18	125	48	24	414	0	1	82	0	5	82	521	

Abreviations: Cm = Calcitic cement / clay matrix, Sor. = sorted, P- M- W = poorly, moderate and well sorted, Ro. = roundness, Sub-a = sub-angular grains, Sub-r = sub-rounded grains, r = rounded grains, Ma = mature, SubMa = submature, InMa = inmmature. * = Noncarbonate extrabasinal grains (NCE), ** = Carbonatic extrabasinal components (CE), *** = Carbonatic intrabasinal components (CI). The mainly parameters are in bold.

Table 4
Percentage of the point-counting data.

Sample	Texture				Framework (%)																			Qmo/Qmr	Qm/Qp	P/F
	Granulometry	Maturity	Disposition		NCE (%)																		Other paritcular components			
					Q (%)						F (%)		Lt (%)			Ch										
			Ro.	Sor.	Qt	Qmo	Qmr	Qp2-3	Qp>3	Cq	K	P	Lm	Lv	Ls	(%)	CE	CI	M	HM	Cm					
Cañón De Caballeros Formation																										
CC-64-01 (Um)	Medium	InMa	r	P	42	11	12	7	5	9	18	4	5	22	1	6	0	0	10	2	27	0.91	2.66	0.19		
CC-64-02a(Um)	Fine	SubMa	Sub-a	P	54	7	43	1	2	0	26	3	3	5	3	6	1	0	14	0	48	0.17	13.67	0.11		
CC-64-02b(Um)	Fine	InMa	Sub-a	P	51	1	42	2	6	0	23	1	2	10	4	8	0	0	6	0	47	0.03	5.41	0.06		
CC-64-03a(Lm)	Coarse	Ma	Sub-r	W	48	8	20	6	15	0	13	2	6	21	6	3	1	0	7	3	9	0.40	1.32	0.14		
CC-64-03b(Lm)	Coarse	SubMa	Sub-r	M	43	6	15	12	10	0	11	1	1	19	11	14	2	0	5	0	20	0.44	0.97	0.09		
CC-64-04 (Lm)	Coarse	SubMa	Sub-a	M	51	11	17	7	12	4	10	4	4	20	7	5	3	0	5	2	16	0.63	1.65	0.27		
Mean ($\bar{x}$)					47.8	7.3	22.5	6.0	8.6	3.2	15.3	3.7	5.9	14.5	6.9	6.2	1.8	0.1	6.4	1.1	25.9	0.42	3.36	0.20		
Vicente Guerrero Formation																										
EMA1-04 (Um)	Coarse	SubMa	Sub-a	M	44	1	28	9	6	0	32	1	3	11	3	7	0	0	14	3	24	0.05	1.9	0.03		
EMA1-05 (Lm)	Fine	InMa	Sub-a	M	49	13	26	9	2	0	20	4	2	2	20	3	3	6	8	2	20	0.50	3.7	0.16		
EMA1-07 (Um)	Fine	InMa	Sub-a	M	50	12	16	15	2	5	29	1	2	5	9	3	0	0	12	4	16	0.73	1.9	0.05		
EMA2-10 (Lm)	Medium	Ma	Sub-r	W	57	12	22	10	7	4	18	1	4	10	7	4	0	0	10	3	14	0.54	2.2	0.05		
CC-54-14 (Lm)	Medium	Ma	Sub-r	W	58	15	25	11	8	0	16	0	1	7	15	1	0	0	0	2	17	0.58	2.1	0.03		
CC-54-15 (Lm)	Medium	Ma	Sub-r	W	55	16	22	10	7	0	19	1	1	8	13	3	0	0	9	2	14	0.72	2.3	0.04		
Mean ($\bar{x}$)	Fine	Ma	Sub-a	M	52.9	9.3	26.2	9.5	3.9	4.0	26.3	1.5	2.5	5.6	6.9	4.3	0.7	0.3	7.1	2.6	19.1	0.38	3.65	0.05		
Del Monte Formation																										
EMA1-01	Medium	InMa	a	P	34	10	12	3	5	3	22	16	4	14	8	4	1	1	7	0	16	0.91	3.1	0.42		
EMA1-02	Medium	InMa	Sub-r	M	30	10	12	2	3	3	22	17	2	14	13	2	6	0	9	1	18	0.77	5.2	0.44		
EMA2-06	Fine	SubMa	a	M	33	7	15	5	2	3	25	20	1	13	6	3	0	0	12	3	22	0.50	3.4	0.44		
EMA2-07	Coarse	SubMa	Sub-r	M	30	8	13	1	5	3	24	19	1	9	17	0	7	0	10	2	17	0.58	3.6	0.44		
EMA2-09	Coarse	SubMa	Sub-a	M	34	8	17	2	4	4	19	8	3	14	22	0	13	0	1	1	23	0.45	5.6	0.29		
CP-207-07	Coarse	SubMa	Sub-a	P	36	12	10	3	4	3	17	13	7	21	9	2	0	3	4	2	18	1.23	3.5	0.44		
Mean ($\bar{x}$)	Medium	SubMa	Sub-r	P	35.0	7.8	14.7	3.0	3.8	5.3	21.1	15.4	4.1	9.6	11.2	4.0	4.1	1.1	5.7	2.1	22.2	0.59	4.70	0.42		
Guacamaya Formation																										
EMA1-14	Coarse	SubMa	Sub-r	M	26	3	12	6	2	3	12	13	11	23	13	2	4	2	5	1	14	0.25	2.1	0.51		
EMA1-15	Coarse	SubMa	Sub-a	M	23	2	13	2	3	3	15	16	3	31	10	1	4	4	4	1	15	0.19	3.8	0.53		
EMA2-01	Corse	Ma	Sub-r	M	29	3	14	5	3	4	15	15	2	24	14	2	5	2	2	0	18	0.19	2.5	0.51		
EMA2-02	Coarse	Ma	Sub-r	M	28	5	16	2	3	2	13	18	3	30	6	1	0	0	1	1	13	0.34	5.5	0.58		
CC34-08	Coarse	InMa	Sub-r	P	30	5	12	3	4	7	22	22	7	8	3	7	0	0	1	1	20	0.38	3.4	0.50		
CP197-03	Coarse	Ma	Sub-r	M	25	6	11	3	4	2	11	12	4	30	12	6	0	3	4	1	16	0.49	2.8	0.51		
Mean ($\bar{x}$)	Coarse	Ma	Sub-r	W	32.5	4.5	13.8	3.8	4.0	6.4	16.5	15.2	3.4	18.8	6.5	7.0	1.3	0.9	2.6	0.7	24.0	0.34	3.67	0.48		

Abreviations: Cm = Calcitic cement / clay matrix, Sor. = sorted, P- M- W = poorly, moderate and well sorted, Ro. = roundness, Sub-a = sub-angular grains, Sub-r = sub-rounded grains, r = rounded grains, Ma = mature, SubMa = submature, InMa = inmmature. * = Noncarbonate extrabasinal grains (NCE), ** = Carbonatic extrabasinal components (CE), *** = Carbonatic intrabasinal components (CI). The mainly parameters are in bold.

Table 5
Recalculated modal and ternary index data.

Samples	Qt–F–L+Ch (%)			Qt–F–L (%)			Qm–F–Lt (%)			Qm–K–P (%)			Lm–Lv–Ls (%)			Qp–Lv–Ls (%)		
	[03]			[04] [05]			[04]			[06]			[03], [05]					
	Qt	F	Lt+Ch	Qt	F	Lt	Qm	F	Lt	Qm	K	P	Lm	Lv	Ls	Qp	Lv	Ls
Cañón de Caballeros Formation																		
CC64-01 (Um)	42	23	35	45	24	31	37	28	35	57	34	8	19	76	5	50	47	3
CC64-02a(Um)	54	29	17	59	32	9	56	32	12	64	33	4	22	35	43	53	21	26
CC64-02b(Um)	51	24	25	55	26	18	51	29	20	64	34	2	14	61	25	56	31	13
CC64-03a(Lm)	48	15	36	51	16	33	36	20	43	64	31	5	17	60	23	52	35	13
CC64-03b(Lm)	43	12	45	51	15	34	33	19	48	63	34	3	4	56	39	54	27	19
CC64-04 (Lm)	51	14	36	56	15	29	42	18	40	70	22	8	11	56	32	48	33	19
Mean (□)	46.6	19.0	33.4	52.3	20.7	26.9	41.3	23.7	35.0	63.5	29.1	7.4	19.5	48.3	32.2	52.5	28.6	18.9
Confidence (-95%)	44.6	15.6	28.2	48.9	17.2	21.5	36.3	20.7	27.7	61.0	25.7	4.7	10.7	35.1	22.8	47.0	20.3	13.1
Confidence (+95%)	50.7	22.4	38.6	55.8	24.3	32.4	46.3	26.8	42.3	66.0	32.5	10.1	28.2	61.6	41.6	58.0	36.9	24.7
Confidence (-99%)	43.3	14.1	26.0	47.4	15.6	19.2	34.2	19.4	24.6	60.0	24.3	3.6	7.0	29.5	18.8	44.6	16.8	10.7
Confidence (+99%)	52.1	23.8	40.8	57.2	25.8	34.7	48.4	28.0	45.4	67.0	33.9	11.2	31.9	67.1	45.6	60.4	40.4	27.2
Vicente Guerrero Formation																		
EMA1-04 (Um)	44	33	23	47	35	17	37	42	21	47	51	2	15	64	21	62	28	9
EMA1-05 (Lm)	49	23	27	59	28	13	50	30	20	63	31	6	6	4	89	32	3	65
EMA1-07 (Um)	50	30	20	52	31	17	41	38	21	52	46	2	14	30	55	61	14	25
EMA2-10 (Lm)	57	19	24	59	20	21	50	24	26	67	31	2	20	48	33	60	23	16
CC-54-14 (Lm)	58	17	25	59	17	24	50	21	30	70	29	1	6	31	63	49	17	34
CC-54-15 (Lm)	55	20	25	57	20	23	48	24	28	66	33	1	6	34	60	50	18	32
Mean (□)	52.8	27.8	19.4	56.0	29.5	14.5	48.1	33.8	18.1	58.9	38.9	2.2	15.7	36.3	48.0	60.1	15.9	24.0
Confidence (-95%)	50.5	25.2	16.9	53.7	26.8	11.9	45.5	31.1	15.1	56.1	36.4	1.5	10.4	27.7	37.9	54.9	12.5	17.4
Confidence (+95%)	55.2	30.3	21.9	58.4	32.2	17.1	50.7	36.4	21.2	61.6	41.5	2.9	20.9	45.0	58.2	65.2	19.4	30.6
Confidence (-99%)	49.6	24.3	16.0	52.8	25.8	11.0	44.6	30.1	14.0	55.1	35.5	1.3	8.5	24.5	34.2	53.1	11.3	15.0
Confidence (+99%)	56.0	31.3	22.8	59.3	33.1	18.0	51.6	37.4	22.2	62.6	42.4	3.1	22.8	48.1	61.8	67.1	20.6	33.0
Del Monte Formation																		
EMA1-01	34	38	29	36	40	24	28	44	28	39	35	25	13	47	40	37	34	29
EMA1-02	30	39	32	33	43	24	27	42	32	39	34	27	6	38	56	21	32	48
EMA2-06	33	45	22	34	46	20	28	50	22	36	36	28	4	66	30	37	43	20
EMA2-07	30	42	28	33	47	20	25	45	30	36	36	28	3	25	72	17	21	61
EMA2-09	34	26	40	41	32	27	30	28	42	52	34	14	5	25	70	13	23	64
CP-207-07	35	28	37	37	30	33	28	34	38	45	31	24	18	51	31	33	42	25
Mean (□)	34	36	30	39	40	21	32	41	27	43	33	24	15	33	52	38	22	40
Confidence (-95%)	31.9	33.4	25.9	35.9	37.8	16.8	28.4	38.3	22.8	40.5	31.0	22.3	9.3	24.3	40.6	29.1	16.6	29.0
Confidence (+95%)	37.1	38.6	33.2	41.9	43.2	24.4	34.7	44.0	31.7	46.0	34.9	25.3	20.9	41.3	63.5	47.0	28.0	50.3
Confidence (-99%)	30.9	32.4	24.6	34.8	36.8	15.4	27.3	37.2	21.2	39.5	30.2	21.7	7.2	21.1	36.4	25.8	14.5	25.1
Confidence (+99%)	38.1	39.5	34.5	43.1	44.1	25.8	35.8	45.1	33.4	47.0	35.6	25.8	23.1	44.5	67.7	50.3	30.0	54.2
Guacamaya Formation																		
EMA1-14	26	26	49	28	28	43	20	29	51	40	29	31	20	43	37	32	36	31
EMA1-15	23	31	46	26	35	39	21	35	44	37	29	33	5	58	36	15	52	33
EMA2-01	29	30	41	33	34	34	24	34	42	41	29	30	4	48	48	20	40	40
EMA2-02	28	31	40	29	32	40	25	33	42	43	24	33	8	76	16	19	66	14
CC34-08	30	45	25	33	48	20	27	52	21	34	33	33	38	44	18	64	25	10
CP197-03	25	23	52	28	25	47	22	27	50	45	27	28	9	60	32	27	48	25
Mean (□)	33	32	36	36	35	28	30	38	32	44	29	27	12	61	27	42	39	18
Confidence (-95%)	29.2	28.9	31.8	32.1	32.0	23.2	25.4	34.4	26.5	40.0	26.9	24.8	7.5	52.3	19.5	32.9	31.7	12.4
Confidence (+95%)	35.9	34.5	39.7	40.6	38.4	33.7	34.2	41.0	38.5	47.2	31.6	29.6	16.9	69.2	34.6	51.7	46.8	24.4
Confidence (-99%)	27.9	27.8	30.3	30.5	30.9	21.3	23.7	33.2	24.2	38.6	26.1	23.9	5.7	49.2	16.6	29.4	28.9	10.2
Confidence (+99%)	37.1	35.6	41.2	42.2	39.5	35.6	35.9	42.3	40.7	48.5	32.4	30.4	18.7	72.4	37.4	55.2	49.6	26.7

Recalculated parameters for ternary plots			
	Parameter	Calculation	Meaning
Qt–F–Lt+Ch [03]	Qt%	100 Qt/(Qt+F+Lt+Ch)	Total stable quartz
	F%	100F/(Qt+F+Lt+Ch)	Total feldspar
	Lt+Ch%	100Lt+Ch/(Qt+F+Lt+Ch)	Total unstable lithic fragments + Chert
Qt–F–Lt [04]; [05]	Q%	100Qt/(Qt+F+Lt)	Total stable quartz
	F%	100F/(Qt+F+Lt)	Total feldspar
	Lt%	100Lt/(Qt+F+Lt)	Total unstable lithic fragments
Qm–F–Lt [04]	Qm%	100Qm/(Qm+F+Lt)	Monocrystalline quartz
	F%	100F/(Qm+F+Lt)	Total feldspar
	Lt%	100Lt/(Qm+F+Lt)	Total unstable lithic fragments
Qm–K–P [04]	Qm%	100Qm/(Qm+K+P)	Monocrystalline quartz
	K%	100K/ (Qm+K+P)	K feldspar
	P%	100P/(Qm+K+P)	Plagioclase
Lm–Lv–Ls [03]; [05]	Lm%	100Lm/(Lm+Lv+Ls)	Total metamorphic lithics
	Lv%	100Lv/(Lm+Lv+Ls)	Total igneous lithics
	Ls%	100Ls/(Lm+Lv+Ls)	Total sedimentary lithics
Qp–Lv–Ls [03]; [05]	Qp%	100Qp/(Qp+Lv+Ls)	Polycristalline quartz + Chert + Metamorphic lithics
	Lv%	100Lv/(Qp2+Lv+Ls)	Total igneous lithics
	Ls%	100Ls/(Qp2+Lv+Ls)	Total sedimentary lithics

Table 6
Photmicrographies of thin sections from the Cañón de Caballeros formation (Upper Silurian-Lower Devonian).

Cañón de Caballeros Formation (Upper Silurian-Lower Devonian)			
Photomicrography		Photomicrography	
parallel nicols	crossed nicols	parallel nicols	crossed nicols
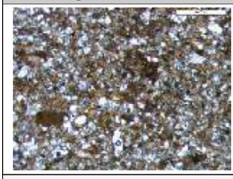	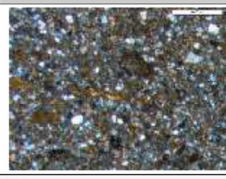	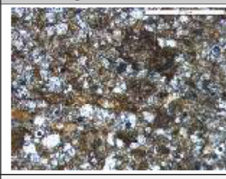	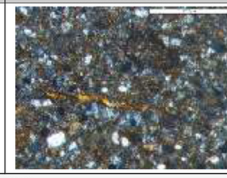
CC64-01		CC64-01	
	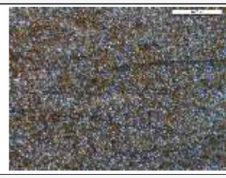		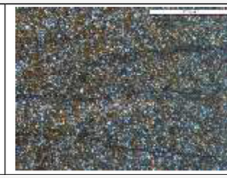
CC64-02a		CC64-02a	
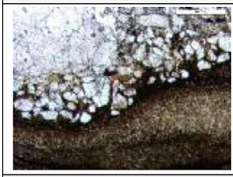	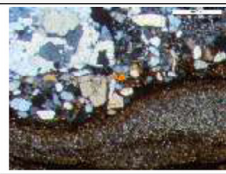		
CC64-02b		CC64-02b	
	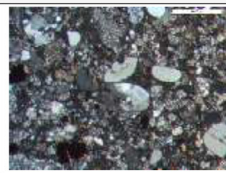		
CC64-03a		CC64-03a	
parallel nicols	crossed nicols	parallel nicols	crossed nicols
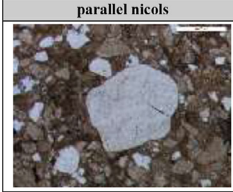	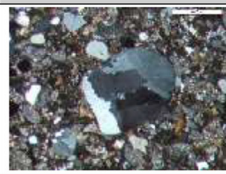		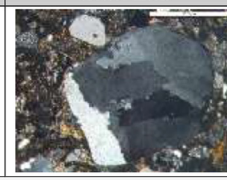
CC64-03b		CC64-03b	
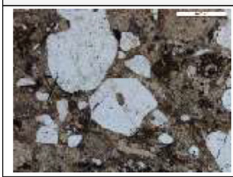	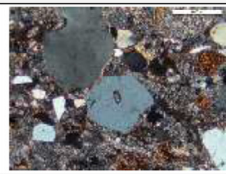	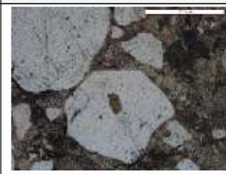	
CC64-04		CC64-04	

Table 7
Photmicrographies of thin sections from the Vicente Guerrero formation (Mississippian).

Vicente Guerrero Formation (Mississippian)			
Photomicrography		Photomicrography	
parallel nicols	crossed nicols	parallel nicols	crossed nicols
	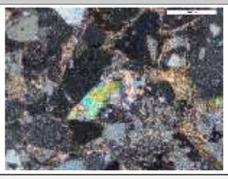		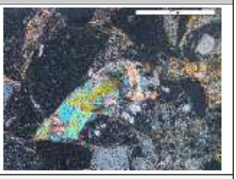
EMA1-04		EMA1-04	
	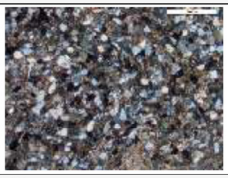		
EMA1-05		EMA1-05	
	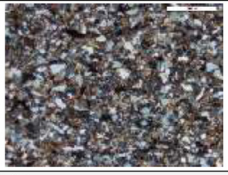		
EMA1-07		EMA1-07	
	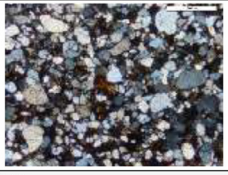	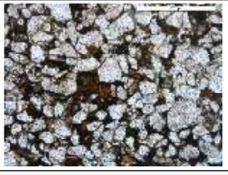	
EMA2-10		EMA2-10	
			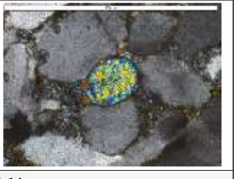
CC54-14		CC54-14	
			
CC54-15		CC54-15	

Table 8
Photmicrographies of thin sections from the Del Monte formation (Pennsylvanian).

Del Monte Formation (Pennsylvanian)			
Photomicrography		Photomicrography	
parallel nicols	crossed nicols	parallel nicols	crossed nicols
	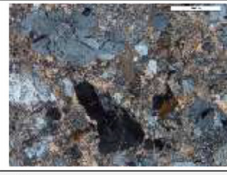		
EMA1-01		EMA1-01	
	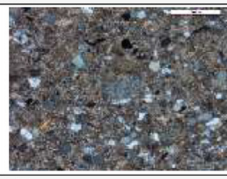	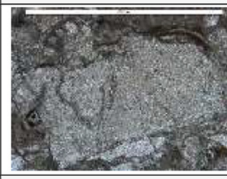	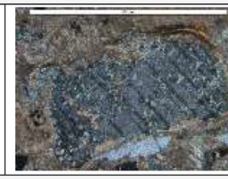
EMA1-02		EMA1-02	
	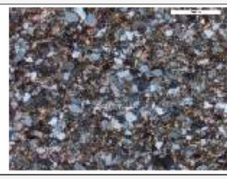		
EMA2-06		EMA2-06	
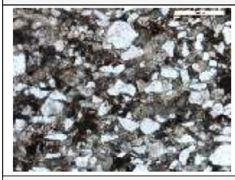			
EMA2-07		EMA2-07	
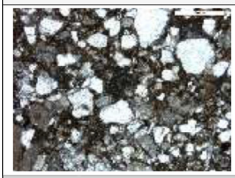			
EMA2-09		EMA2-09	
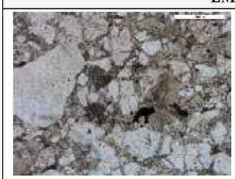	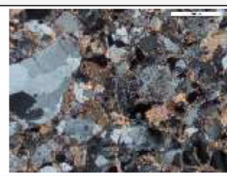	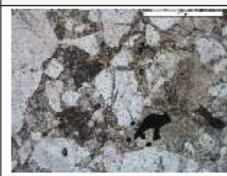	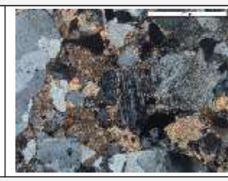
CP207-07		CP207-07	

Table 9
Photmicrographies of thin sections from the Guacamaya formation (Permian).

Guacamaya Formation (Permian)			
Photomicrography		Photomicrography	
parallel nicols	crossed nicols	parallel nicols	crossed nicols
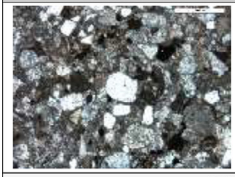	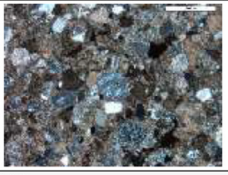		
EMA1-14		EMA1-14	
			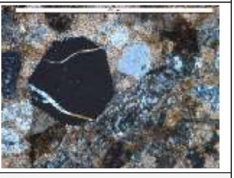
EMA1-15		EMA1-15	
			
EMA2-01		EMA2-01	
	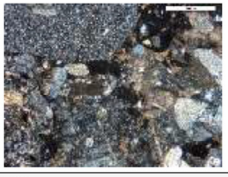		
EMA2-02		EMA2-02	
	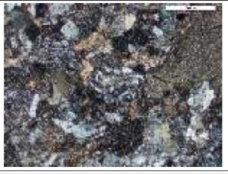		
CC34-08		CC34-08	
		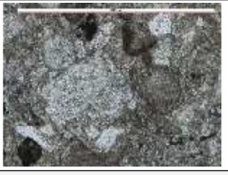	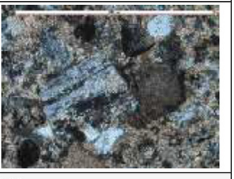
CP197-03		CP197-03	

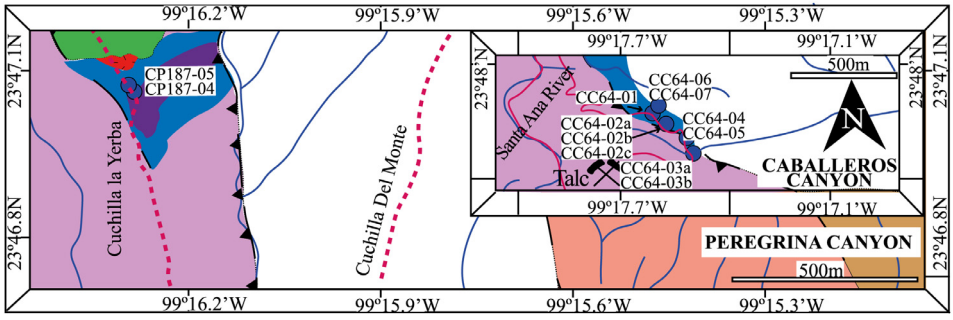

Fig. 8. Sample locations of the Cañón de Caballeros formation (Upper Silurian-Lower Devonian).

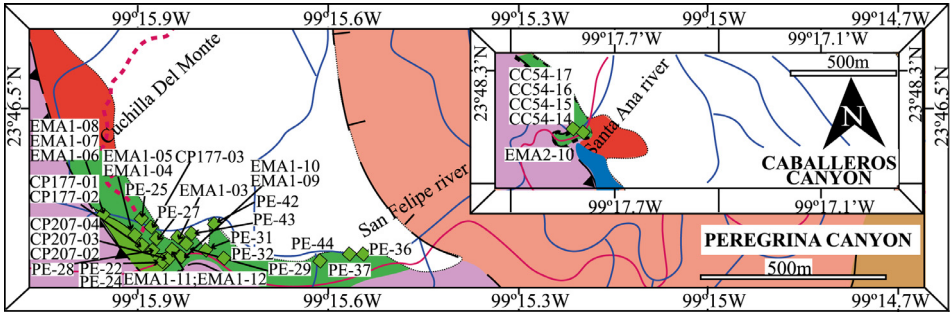

Fig. 9. Sample locations of the Vicente Guerrero formation (Mississippian).

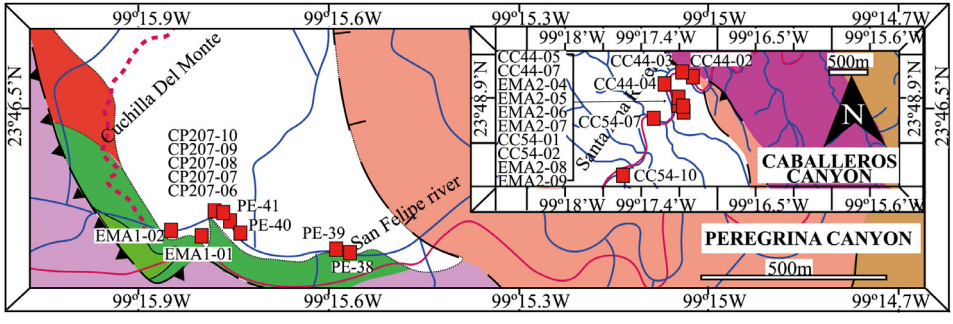

Fig. 10. Sample locations of the Del Monte formation (Pennsylvanian).

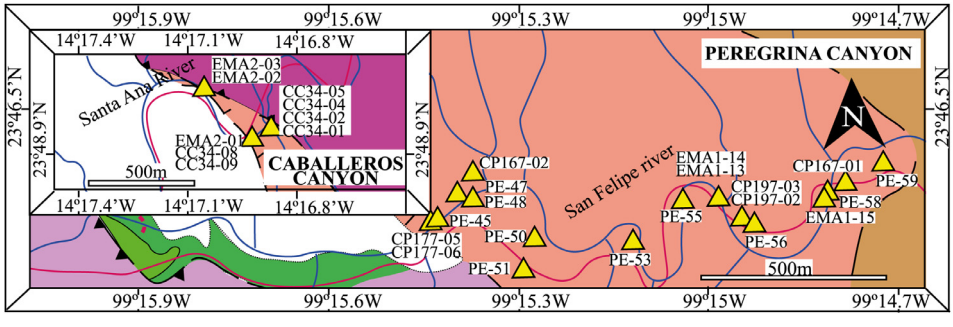

Fig. 11. Sample locations of the Guacamaya formation (Permian).

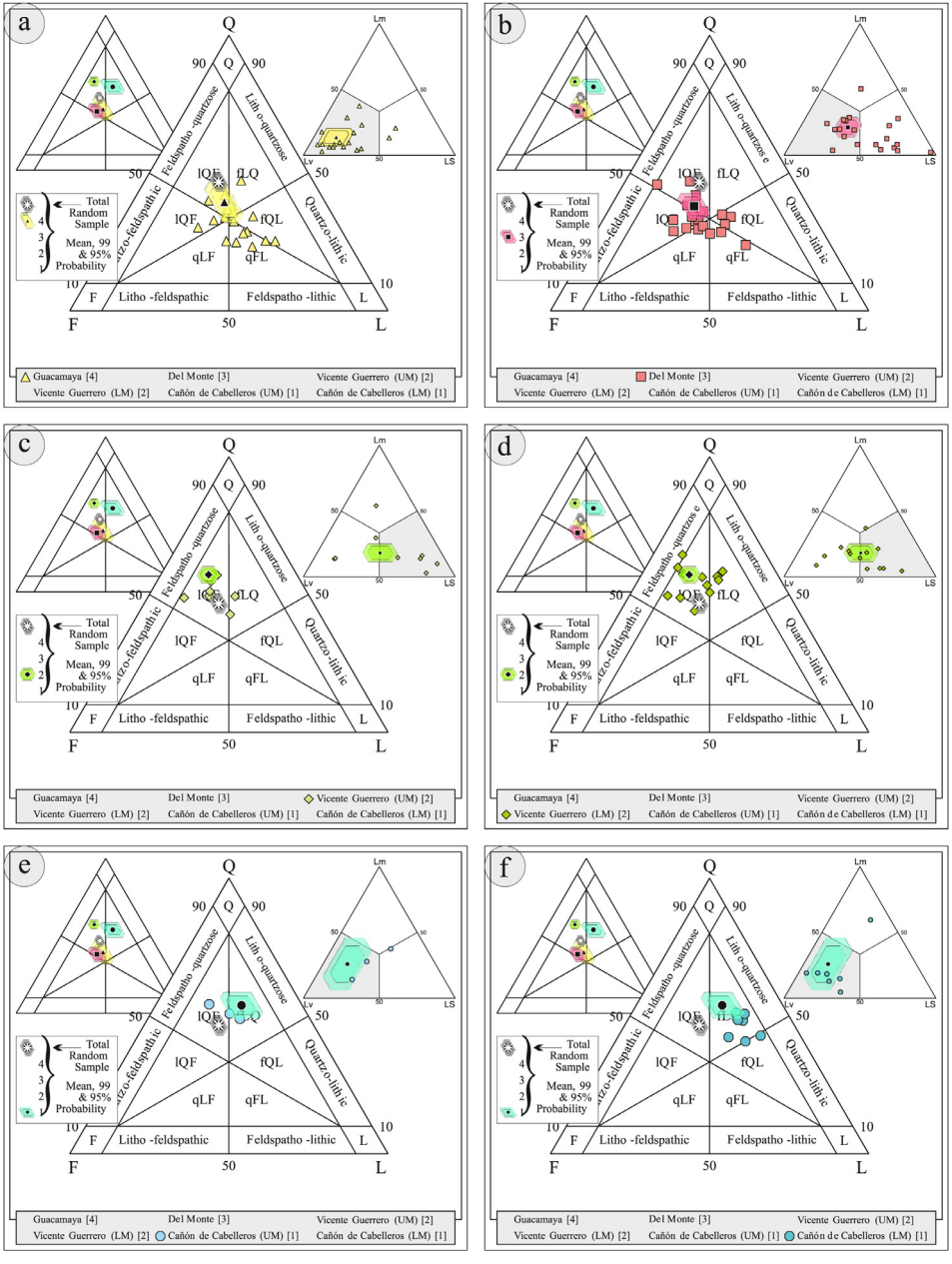

Fig. 12. Petrographic modal analysis of Tamatán Group sandstones: Q–F–L after [8].

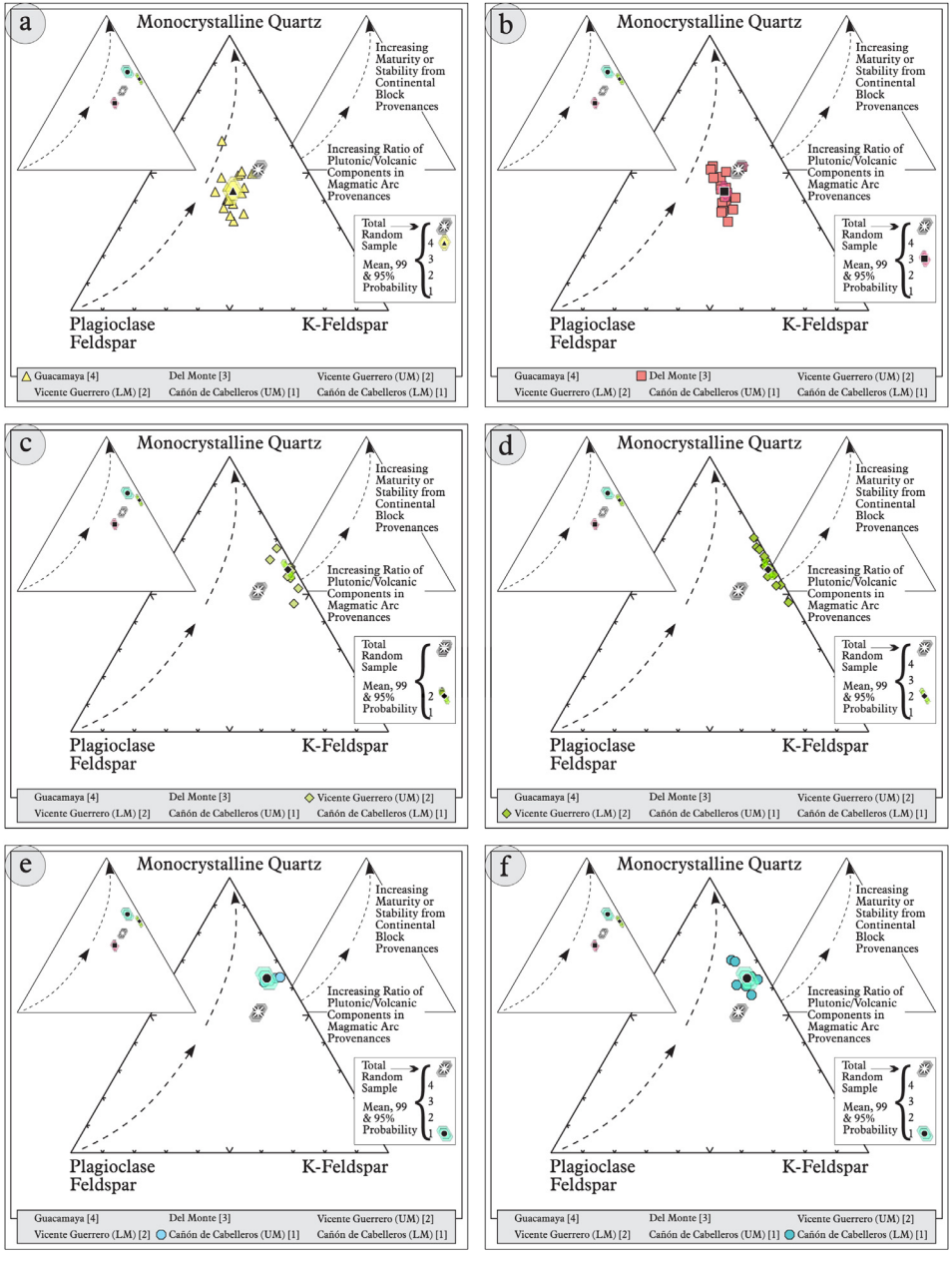

Fig. 13. Petrographic modal analysis of Tamatán Group sandstones: Qm–P–K after [6].

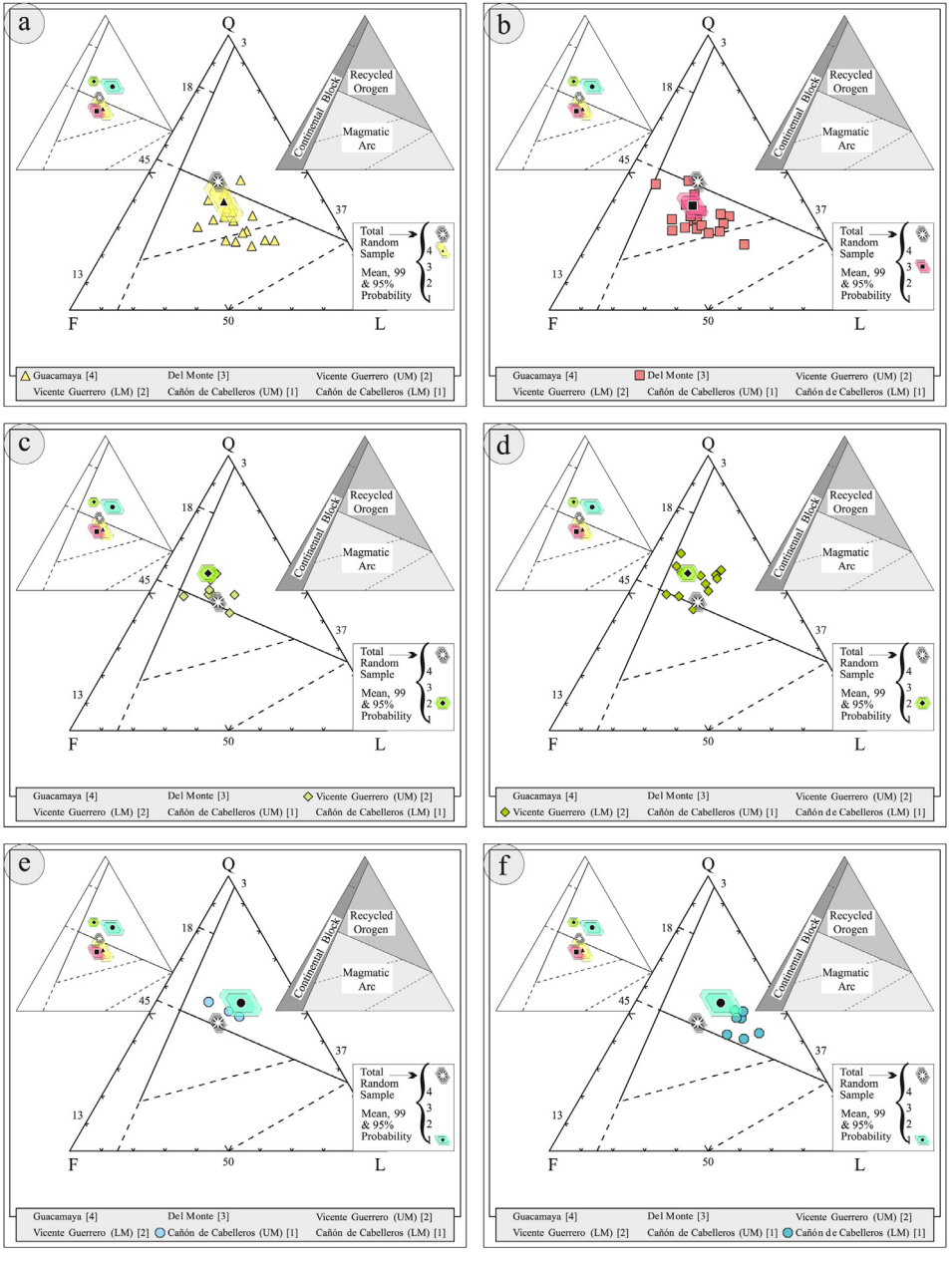

Fig. 14. Petrographic modal analysis of Tamatán Group sandstones: Q–F–L after [4].

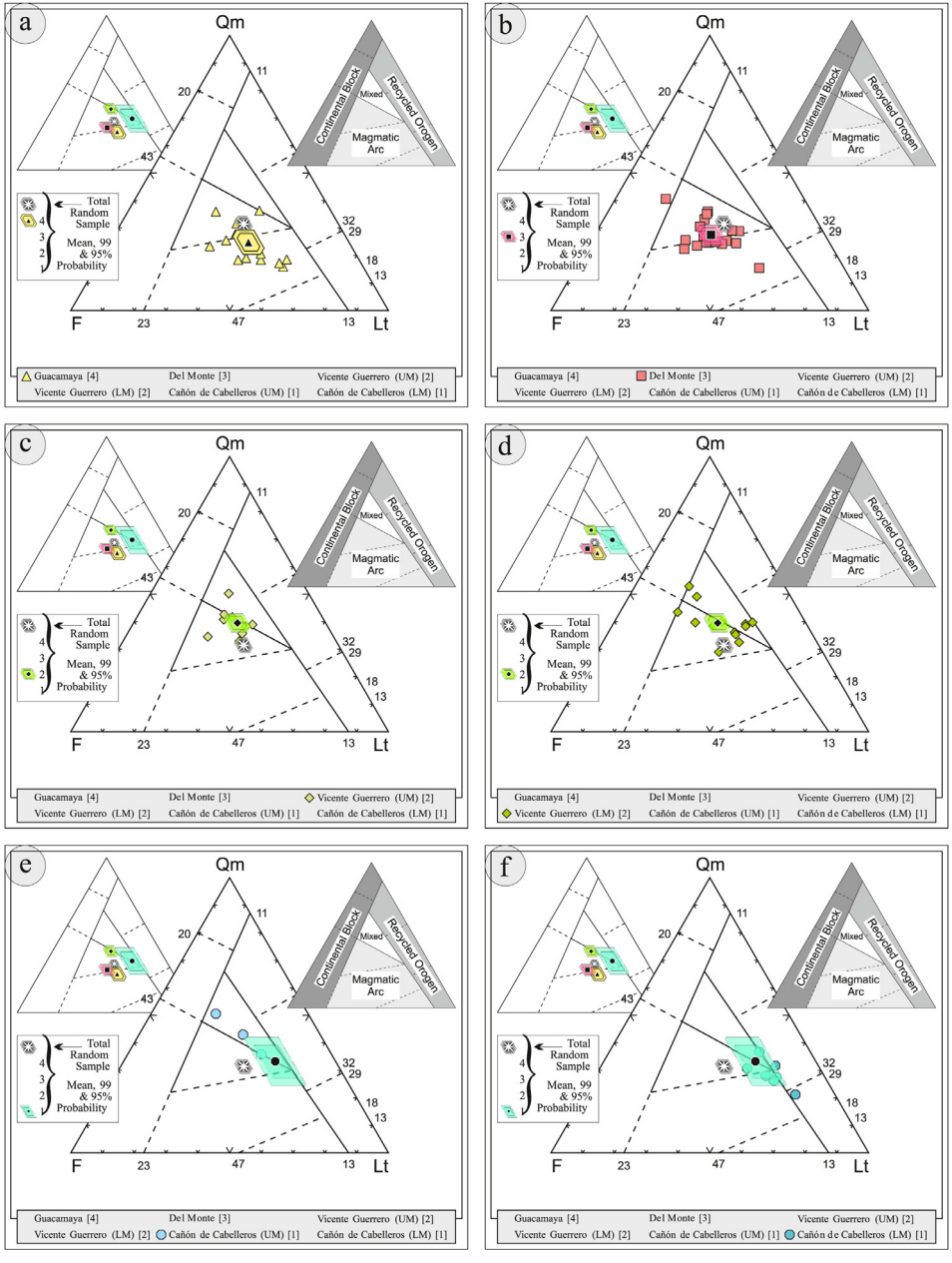

Fig. 15. Petrographic modal analysis of Tamatán Group sandstones: Qm–F–Lt after [9].

4.3. Geochemical data

Tables 10-13, Figs. 16-24.

Table 10
Geochemical parameters of selected samples from the Cañon de Caballeros and Vicente Guerrero formations.

	Cañón de Caballeros Formation						Vicente Guerrero Formation					
Sample	CC64-01	CC64-02a	CC64-02b	CC64-03a	CC64-03b	CC64-04	EMA1-04	EMA1-05	EMA1-07	EMA2-10	CC54-14	CC54-15
SiO2	70,21	73,15	74,21	77,66	76,59	75,27	65,83	71,13	62,9	84,4	80,23	84,51
TiO2	0,36	1,06	0,93	0,51	0,53	0,52	0,22	0,61	0,57	0,74	0,63	0,78
Al2O3	14,9	11,1	10,45	8,95	9,47	9,12	15,65	8,34	10,19	5,49	5,94	5,97
Fe2O3	4,15	6,43	6,62	5,09	5,49	5,52	7,55	3,22	7,01	5,26	8,5	4,65
MnO	0,03	0,01	0,02	0,04	0,06	0,08	0,03	0,09	0,13	0,02	0,04	0,02
MgO	1,35	0,86	0,87	1,69	1,75	1,84	1,55	0,88	3,39	0,73	1,17	0,66
CaO	0,14	0,11	0,09	0,51	0,22	1,18	0,74	6,14	4,55	0,25	0,23	0,06
CaO*	0,09	0,02	0	0,32	0,05	0,87	0,5	0,78	0,25	0,1	0,15	0
Na2O	0,05	0,05	0,05	0,03	0,04	0,04	0,08	0,6	0,07	0	0,26	0,04
K2O	3,84	2,13	1,83	2,09	2,22	2,11	3,63	1,91	2,33	0,77	0,36	1,01
P2O5	0,04	0,08	0,08	0,1	0,14	0,12	0,07	0,08	0,09	0,09	0,07	0,09
LOI	4,7	4,9	4,7	3	3,1	3,8	4,5	6,9	8,6	2,1	2,5	2,1
CO2	n.d.	n.d.	n.d.	0,29	n.d.	0,43	0,48	4,96	6,7	0,15	n.d.	n.d.
CaCO3*	n.d.	n.d.	n.d.	0,12	n.d.	0,3	0,29	9,41	7,48	0,07	n.d.	n.d.
Cr	13	75	61	20	20	20	20	82	68	34	34	41
Ni	7	35	38	9	11	10	23	15	23	9	9	7
Co	2	8	10	5	7	6	4	3	7	3	4	2
Sc	3	9	7	5	5	5	4	6	9	4	5	4
V	32	70	59	50	42	38	23	73	113	95	74	77
Pb	15	2	2	6	5	4	5	1	1	1	4	4
Zn	165	47	45	112	204	348	47	21	38	36	66	52
Rb	103	72	64	65	70	67	80	61	67	19	8	22
Ba	715	333	295	624	653	719	456	296	291	185	78	147
Sr	10	9	8	8	8	9	15	94	32	17	13	10
Ga	31	14	13	19	21	19	17	11	11	8	7	7
Ta	4,5	1	0,9	5,3	5,8	5,4	1,6	0,9	0,5	0,9	0,5	0,7
Nb	79	15,4	14,4	85	90,7	83,6	19,8	9,3	8,8	18,8	11,4	13,4
Hf	15,9	9,4	7,1	28,9	31	29,5	4,4	5,6	6,6	14,8	10,3	13,7
Zr	460	357	266	1114	1223	1158	116	232	222	579	426	566
Y	91	24	19	107	116	108	24	14	16	15	10	12
Th	14,1	7,1	6	17,3	18,6	17,6	4,6	5,8	5,4	4,8	3,6	4,5
U	3,3	2,2	1,6	4,2	4,2	4,1	2,2	1	0,8	0,9	0,9	1,1
La	73,9	29,1	20,6	70,9	76,5	89,8	21,5	19	19	18,3	15	17,5
Ce	135,7	60,7	41,4	165,7	175,2	210,7	41,6	39,5	41,5	38,5	24,8	35,4
Pr	18,18	7,3	4,86	17,28	18,44	22,02	4,97	4,82	4,88	4,63	2,49	4,22
Nd	71	28,7	18	65,5	71,1	85,1	17,8	20,5	18,6	16,6	8,9	16,2
Sm	16,16	5,32	3,43	15,2	16,24	19,73	4,07	4,09	4,08	3,96	1,4	2,92
Eu	1,1	1,12	0,74	1,69	1,74	2,19	0,73	0,81	0,95	0,72	0,35	0,67
Gd	17,28	4,26	3,2	15,25	16,45	17,97	3,95	3,42	3,83	3,16	1,35	2,39
Tb	2,91	0,69	0,54	2,75	3,02	2,96	0,68	0,55	0,59	0,53	0,23	0,38
Dy	17,15	4,28	3,43	17,43	19,3	18,23	4,37	2,96	3,32	3,11	1,72	2,21
Ho	3,54	0,91	0,74	3,97	4,27	3,87	0,92	0,62	0,7	0,48	0,38	0,49
Er	10,31	2,86	2,32	12,01	13,37	12,28	1,99	1,81	1,66	1,51	1,49	1,53
Tm	1,53	0,44	0,35	1,89	2,04	1,9	0,41	0,27	0,28	0,31	0,21	0,24
Yb	10,24	2,81	2,53	12,41	13,84	12,82	2,07	1,71	1,66	1,85	1,48	1,65
Lu	1,52	0,44	0,38	1,94	2,17	2	0,36	0,23	0,26	0,28	0,25	0,26
Chem.Lit	Rest++	Psam.it	Psam.	Psam.	Psam.	Psam.	Pelite	CaO++	Rest--	Psam.	Psam.	Psam.
Zr/Ti	1278	337	286	2186	2308	2228	530	381	390	784	677	726
Nb/Y	0,86	0,63	0,72	0,79	0,77	0,77	0,79	0,65	0,52	1,24	1,04	1,04
Th/Sc	4,7	0,78	0,85	3,46	3,72	3,52	1,14	0,96	0,6	1,2	0,72	1,12
Ti/Nb	27	413	387	36	35	37	67	393	388	236	331	349
CIA	77	82	84	76	79	70	76	65	77	84	85	84
PIA	98	99	99	91	98	81	92	72	93	96	89	99
CIW	98	99	99	93	98	85	94	78	95	97	90	99
Eu/Eu*	0,2	0,72	0,68	0,34	0,33	0,36	0,56	0,66	0,73	0,62	0,78	0,78
REE	4,88	7	5,5	3,86	3,74	4,73	7,02	7,51	7,73	6,68	6,85	7,17
LREE	2,87	3,44	3,78	2,93	2,96	2,86	3,32	2,92	2,93	2,9	6,74	3,77
HREE	1,36	1,22	1,02	0,99	0,96	1,13	1,54	1,62	1,86	1,38	0,73	1,17
∑-REE	380,52	148,93	102,52	403,92	433,68	501,57	105,42	100,29	101,31	93,94	60,05	86,06

Note: Oxides and LOI in %, other elements in ppm. Abbreviations: n.d.: not detected; CaCO* = maximum CaO in Carbonates recalculated from CO_2; Chem.Lit: Chemical lithology [10]; CaO++: CaO enriched samples; Psam.: Psammite classified samples; Rest++: enriched in SiO_2 and Al_2O_3; Rest−: impoverished in SiO_2 and Al_2O_3;. Eu/Eu*=$Eu_N/(Sm_N x Gd_N)^{0.5}$; REE= La_N/ Lu_N; LREE=La_N/Sm_N; HREE=Gd_N/ Lu_N; ∑-REE= Total REE (in ppm); Samples are not LOI-free recalculated.

Table 11
Geochemical parameters of selected samples from the Vicente Guerrero and Del Monte formations.

	Del Monte Formation						Guacamaya Formation					
Sample	**EMA1-01**	**EMA1-02**	**EMA2-06**	**EMA2-07**	**EMA2-09**	**CP-207-07**	**EMA1-14**	**EMA1-15**	**EMA2-01**	**EMA2-02**	**CC-34-08**	**CP-197-03**
SiO2	50,23	37,57	56,53	50,01	48,29	51,44	40,88	35,27	55,58	53,73	59,56	62,46
TiO2	0,33	0,21	0,5	0,25	0,25	0,17	0,53	0,39	0,51	0,67	0,45	0,72
Al2O3	10,3	7,42	11,73	9,86	7,96	8,07	10,08	8,93	17,27	16,72	16,53	9,64
Fe2O3	2,26	1,64	4,96	2,14	2,03	2,25	6,85	8,08	4,92	6,47	4,9	7,32
MnO	0,05	0,06	0,04	0,06	0,09	0,04	0,19	0,17	0,12	0,14	0,1	0,08
MgO	1,95	1,85	3,21	1,71	1,55	0,82	2,52	6,28	2,72	3,47	2,78	2,09
CaO	15,78	26,01	8,78	16,21	19,42	18,08	19,18	17,29	5,31	5,49	3,9	6,95
CaO*	0,11	1,52	2,85	1,79	1,61	1,94	2,25	0,97	2,22	2,56	2,32	2,39
Na2O	1,9	1,27	2,24	2,18	2,11	2,04	2,01	1,2	7,13	4,93	5,41	2,18
K2O	2,07	1,64	2,24	2,3	1,51	1,96	0,4	0,55	0,5	1,5	1,16	0,36
P2O5	0,09	0,07	0,2	0,13	0,12	0,05	0,04	0,08	0,09	0,12	0,07	0,09
LOI	14,9	22,1	9,4	14,9	16,5	15	17,2	21,6	5,7	6,6	5	8
CO2	14,31	21,05	6,74	12,84	15,41	13,42	15,67	19,17	4	4,12	2,34	4,95
CaCO3*	27,77	43,57	10,16	25,47	31,54	28,7	30,13	28,97	5,32	4,98	2,68	7,94
Cr	34	27	41	27	41	27	0	27	27	27	20	34
Ni	8	11	20	10	9	6	14	8	5	6	4	19
Co	3	3	6	5	3	2	10	9	9	16	10	15
Sc	7	4	8	7	6	4	15	12	18	26	19	15
V	30	18	52	25	18	20	111	72	101	131	93	112
Pb	10	10	13	10	6	5	8	11	12	8	10	14
Zn	36	88	75	57	24	34	82	38	62	50	128	46
Rb	65	45	59	68	42	55	11	13	11	32	26	9
Ba	443	314	745	8	600	306	110	121	125	400	224	159
Sr	266	337	199	425	451	321	234	152	161	251	108	99
Ga	10	7	12	10	8	7	9	8	14	14	16	7
Ta	0,2	0,1	0,3	0,2	0,3	0,1	0,2	0,1	0,2	0,3	0	0,2
Nb	3,5	2,9	5,2	3,1	2,5	2,1	2,9	0,7	1,8	2,5	2	2,4
Hf	4,1	2,2	3,4	2,9	3,3	2,2	1,7	0,9	1,9	2,5	1,6	1,3
Zr	131	93	126	115	95	77	49	35	60	77	60	51
Y	15	15	18	15	23	13	23	15	16	22	16	13
Th	3,5	2,3	3,6	8,1	5	3,2	1,4	1,2	1,9	2,8	1,9	1
U	0,8	1,4	1,3	1,8	1,7	0,9	0,8	1	0,9	1,3	0,7	0,6
La	14,7	12,7	19,5	17	19,6	14,1	7,5	5,3	6,2	7,8	10,2	6,8
Ce	28,4	23,9	39,5	36	36,6	25,8	14,8	9,9	12,6	19	19,8	11,7
Pr	3,62	3,31	5,05	4,44	4,68	3,17	2,14	1,44	1,88	2,35	2,52	1,61
Nd	14,1	13,1	22,1	18,6	17,4	12,1	11,1	7,5	7,3	10,9	10,8	7,1
Sm	3,37	2,95	4,57	3,64	3,88	2,34	3,35	2,21	2,51	2,92	2,43	1,93
Eu	0,79	0,69	1,12	0,71	0,8	0,61	0,95	0,71	1,03	0,83	1	0,52
Gd	2,99	2,53	4,35	3,11	4,03	2,14	3,95	2,41	2,61	3,37	2,73	2,33
Tb	0,44	0,42	0,68	0,49	0,59	0,33	0,65	0,43	0,48	0,59	0,46	0,37
Dy	2,77	2,69	3,53	2,94	3,71	2,05	3,17	2,73	2,83	3,89	2,8	2,23
Ho	0,6	0,48	0,72	0,58	0,73	0,42	0,65	0,58	0,6	0,97	0,64	0,46
Er	1,46	1,48	1,94	1,5	2	1,28	2,25	1,42	1,87	2,56	1,78	1,3
Tm	0,27	0,22	0,27	0,27	0,29	0,18	0,36	0,21	0,26	0,34	0,27	0,18
Yb	1,57	1,13	1,65	2,05	1,54	1,21	2,27	1,16	1,53	2,71	1,85	1,21
Lu	0,24	0,23	0,26	0,28	0,3	0,19	0,3	0,19	0,25	0,4	0,28	0,2
Chem.Lit	CaO++:	CaO++:	CaO++:	CaO++:	CaO++:	CaO++:	CaO++	CaO++	CaO++	CaO++	Pelite	CaO++
Zr/Ti	398	445	253	461	383	453	93	92	118	116	134	71
Nb/Y	0,22	0,19	0,27	0,2	0,1	0,16	0,12	0,04	0,1	0,1	0,12	0,17
Th/Sc	0,5	0,57	0,45	1,15	0,83	0,8	0,09	0,1	0,1	0,1	0,1	0,06
Ti/Nb	565	434	576	483	600	485	1096	3340	1699	1607	1349	1799
CIA	65	53	51	51	50	47	56	67	51	54	54	54
PIA	71	54	51	52	50	46	57	69	52	54	54	54
CIW	76	61	57	59	55	54	58	71	52	57	56	55
Eu/Eu*	0,76	0,77	0,77	0,64	0,62	0,83	0,8	0,94	1,23	0,81	1,19	0,75
REE	6,33	7,59	7,99	5,6	8,6	7,87	2,23	3,09	2,74	1,94	3,73	3,8
LREE	2,74	2,7	2,68	2,93	3,17	3,79	1,4	1,5	1,55	1,68	2,64	2,21
HREE	1,54	1,81	2,13	1,22	2,12	1,43	1,41	1,68	1,38	1	1,19	1,56
∑-REE	75,32	65,83	105,24	91,61	96,15	65,92	53,44	36,19	41,95	58,63	57,56	37,94

Note: Oxides and LOI in %, other elements in ppm. Abbreviations: n.d.: not detected; CaCO* = maximum CaO in Carbonates recalculated from CO_2; Chem.Lit: Chemical lithology [10]; CaO++: CaO enriched samples; Psam.: Psammite classified samples; Rest++: enriched in SiO_2 and Al_2O_3; Rest−: impoverished in SiO_2 and Al_2O_3;. $Eu/Eu^* = Eu_N/(Sm_N x Gd_N)^{0.5}$; REE= La_N/ Lu_N; LREE=La_N/Sm_N; HREE=Gd_N/ Lu_N; ∑-REE=Total REE (in ppm); Samples are not LOI-free recalculated.

Table 12
Simple statistics of the selected geochemical parameters of the Tamatán Group.

		K_2O (%)	Na_2O (%)	Al_2O_3 (%)	SiO_2 (%)	Cr	SiO_2/K_2O	Ti/Nb	K (%)	Th (ppm)	Th/Sc	Zr/Sc	K_2O/Na_2O	SiO_2/Al_2O_3
Cañón de Caballeros Formation	Mean	2.881	0.048	11.425	73.211	29.650	28.436	127.856	2.392	12.817	2.691	138.615	6.718	59.838
	-95%	2.259	0.041	9.851	71.317	12.027	22.188	20.083	1.875	10.038	1.837	89.719	5.698	50.828
	+95%	3.503	0.055	12.999	75.104	47.273	34.683	235.630	2.908	15.595	3.545	187.510	7.739	68.847
	-99%	2.003	0.038	9.204	70.539	4.782	19.620	-24.222	1.663	8.896	1.486	69.619	5.278	47.124
	+99%	3.759	0.058	13.646	75.883	54.518	37.251	279.935	3.120	16.738	3.896	207.611	8.159	72.551
Vicente Guerrero Formation	Mean	2.143	0.361	9.718	75.141	78.242	47.463	384.68	1.779	5.373	0.751	48.235	8.516	17.944
	-95%	1.803	0.096	8.602	71.717	61.478	30.512	343.36	1.497	4.648	0.637	29.585	7.239	11.646
	+95%	2.482	0.626	10.833	78.565	95.007	64.414	426.00	2.061	6.099	0.866	66.884	9.793	24.242
	-99%	1.683	0.003	8.208	70.507	55.552	24.521	328.76	1.397	4.391	0.596	22.993	6.788	9.420
	+99%	2.602	0.720	11.227	79.775	100.932	70.405	440.60	2.160	6.355	0.906	73.476	10.244	26.468
Del Monte Formation	Mean	2.052	1.664	8.711	46.622	28.646	24.156	501.41	1.704	4.023	0.732	17.937	5.508	1.287
	-95%	1.634	1.395	7.294	41.076	20.919	20.987	443.32	1.357	3.026	0.594	15.569	5.055	0.968
	+95%	2.471	1.932	10.127	52.168	36.373	27.325	559.50	2.051	5.020	0.869	20.305	5.961	1.606
	-99%	1.466	1.287	6.725	38.847	17.814	19.713	419.97	1.217	2.625	0.539	14.617	4.873	0.840
	+99%	2.639	2.040	10.697	54.397	39.479	28.599	582.85	2.191	5.421	0.924	21.256	6.143	1.734
Guacamaya Formation	Mean	1.088	2.836	13.600	56.598	39.428	70.339	1373.44	0.903	2.450	0.153	4.731	4.266	0.473
	-95%	0.729	2.023	12.249	51.626	30.142	50.307	1077.11	0.605	1.960	0.116	3.794	3.791	0.322
	+95%	1.447	3.649	14.951	61.569	48.713	90.370	1669.76	1.201	2.940	0.190	5.669	4.741	0.624
	-99%	0.595	1.719	11.744	49.769	26.673	42.821	966.38	0.494	1.777	0.103	3.443	3.614	0.265
	+99%	1.581	3.953	15.456	63.427	52.183	97.856	1780.49	1.312	3.123	0.204	6.020	4.918	0.680

Table 13
Simple statistics of the rare earth elements (REE) of the Tamatán Group.

		La_N	Ce_N	Pr_N	Nd_N	Sm_N	Eu_N	Gd_N	Tb_N	Dy_N	Ho_N	Er_N	Tm_N	Yb_N	Lu_N
Cañón de Caballeros Formation	Mean	164.464	132.558	105.620	77.579	52.424	14.655	39.066	35.082	34.114	32.883	34.361	36.798	35.524	35.717
	-95%	126.898	99.477	80.849	59.125	38.035	11.565	27.637	24.430	24.080	23.116	24.060	25.768	24.965	25.052
	+95%	202.031	165.639	130.392	96.033	66.814	17.745	50.495	45.733	44.149	42.650	44.661	47.827	46.083	46.383
	-99%	111.454	85.878	70.665	51.538	32.119	10.295	22.938	20.052	19.955	19.101	19.826	21.234	20.625	20.667
	+99%	217.474	179.239	140.576	103.619	72.729	19.015	55.193	50.111	48.274	46.665	48.896	52.361	50.424	50.767
Vicente Guerrero Formation	Mean	53.709	42.939	35.285	26.291	15.525	9.229	9.976	8.404	7.392	6.694	6.707	7.532	6.789	7.019
	-95%	6.958	5.914	4.918	3.804	2.391	1.389	1.470	1.338	1.178	1.080	0.987	1.095	0.885	1.033
	+95%	46.751	37.025	30.367	22.487	13.134	7.840	8.506	7.065	6.214	5.614	5.719	6.437	5.905	5.985
	-99%	9.406	7.994	6.649	5.142	3.232	1.878	1.987	1.809	1.592	1.459	1.335	1.480	1.196	1.397
	+99%	44.303	34.945	28.636	21.149	12.293	7.352	7.989	6.595	5.800	5.234	5.372	6.052	5.593	5.622
Del Monte Formation	Mean	39.384	29.982	26.620	20.729	13.044	8.011	9.090	7.613	6.869	6.273	5.984	6.461	5.661	5.855
	-95%	33.170	25.161	22.486	17.370	10.921	6.756	7.536	6.436	5.854	5.374	5.212	5.620	4.826	-3.922
	+95%	45.598	34.802	30.754	24.089	15.166	9.265	10.644	8.790	7.883	7.172	6.755	7.301	6.496	15.632
	-99%	30.673	23.223	20.824	16.019	10.068	6.251	6.911	5.963	5.447	5.013	4.902	5.283	4.490	-7.851
	+99%	48.095	36.740	32.416	25.439	16.019	9.770	11.269	9.263	8.290	7.533	7.065	7.639	6.832	19.561
Guacamaya Formation	Mean	25.549	20.997	19.223	16.464	12.541	9.182	10.087	8.925	8.055	7.631	7.468	7.634	7.272	7.349
	-95%	20.749	16.400	15.383	13.415	10.721	8.089	8.620	7.742	7.039	6.698	6.578	6.657	6.295	6.453
	+95%	30.349	25.594	23.062	19.513	14.362	10.275	11.553	10.108	9.070	8.564	8.357	8.611	8.249	8.245
	-99%	18.935	14.664	13.933	12.263	10.033	7.676	8.066	7.295	6.656	6.346	6.242	6.287	5.926	6.114
	+99%	32.162	27.330	24.513	20.665	15.049	10.688	12.107	10.555	9.453	8.917	8.693	8.980	8.619	8.584

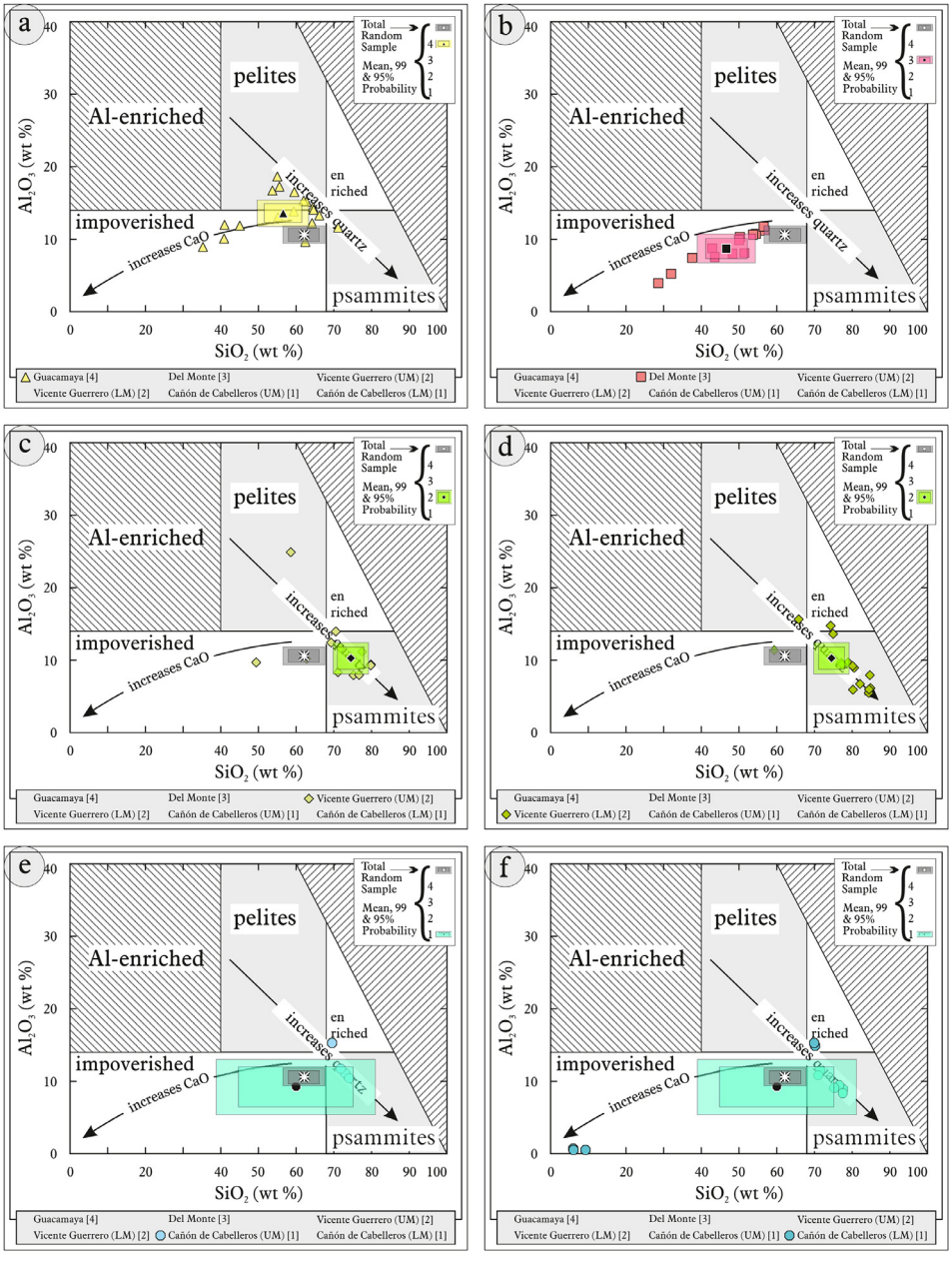

Fig. 16. Geochemical sediment classification of the Tamatán Group: SiO_2–Al_2O_3 diagram after [10].

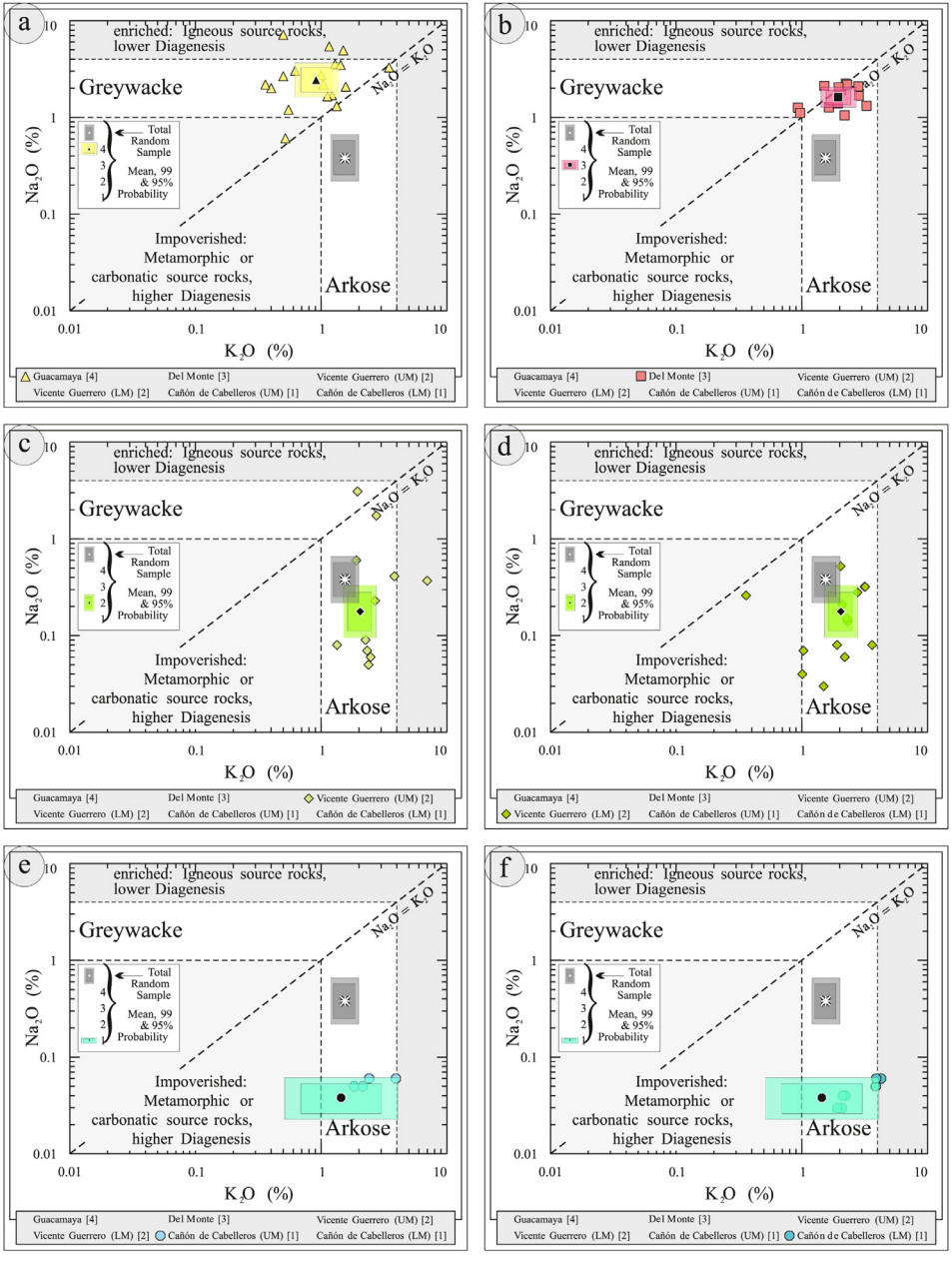

Fig. 17. Geochemical sediment classification of the Tamatán Group: K_2O–Na_2O diagram after [10].

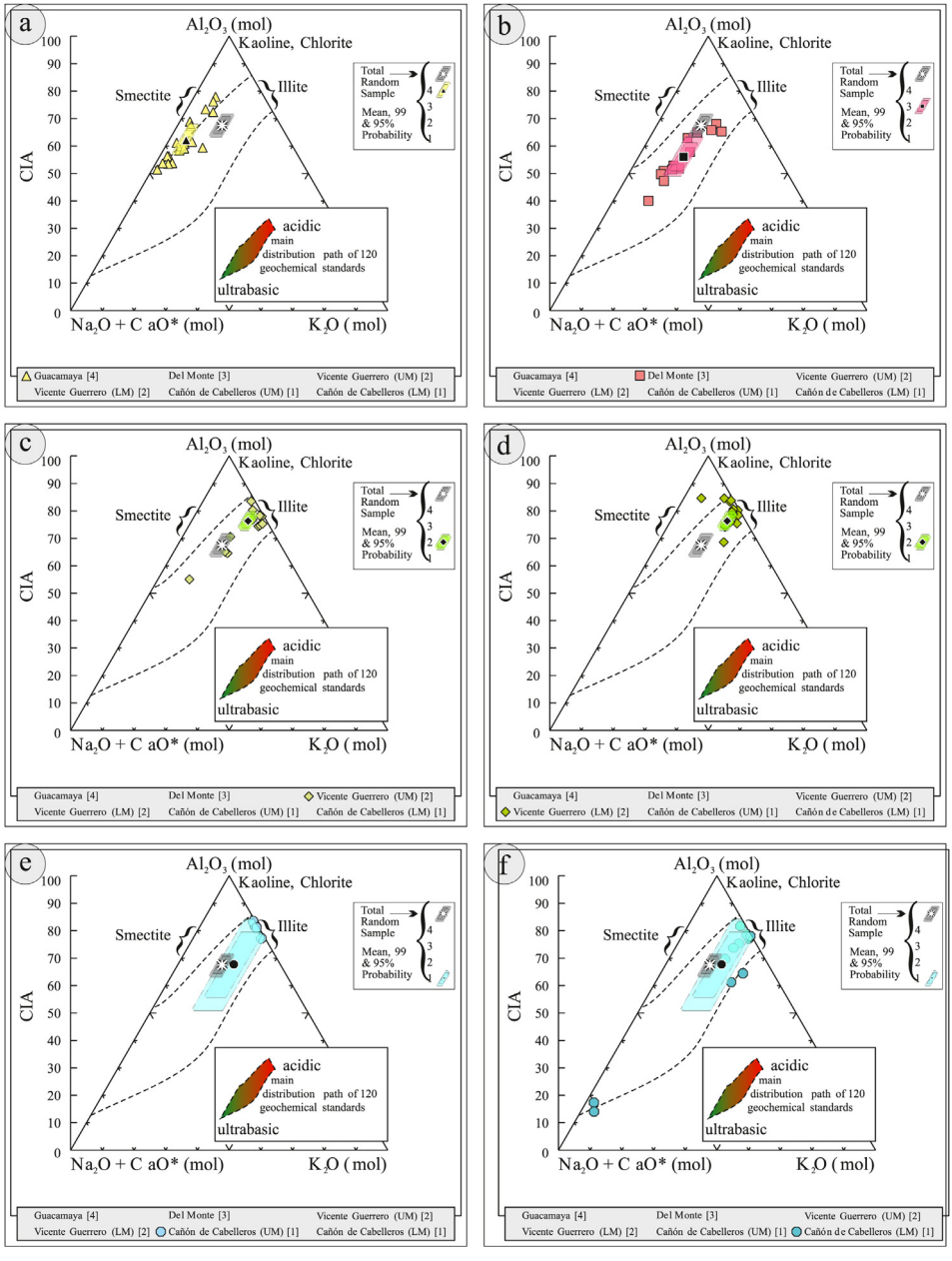

Fig. 18. Geochemical Index of Alteration of the sediments of the Tamatán Group: $Na_2O+CaO–Al_2O_3–K_2O$ diagram after [12,13] modified by [10].

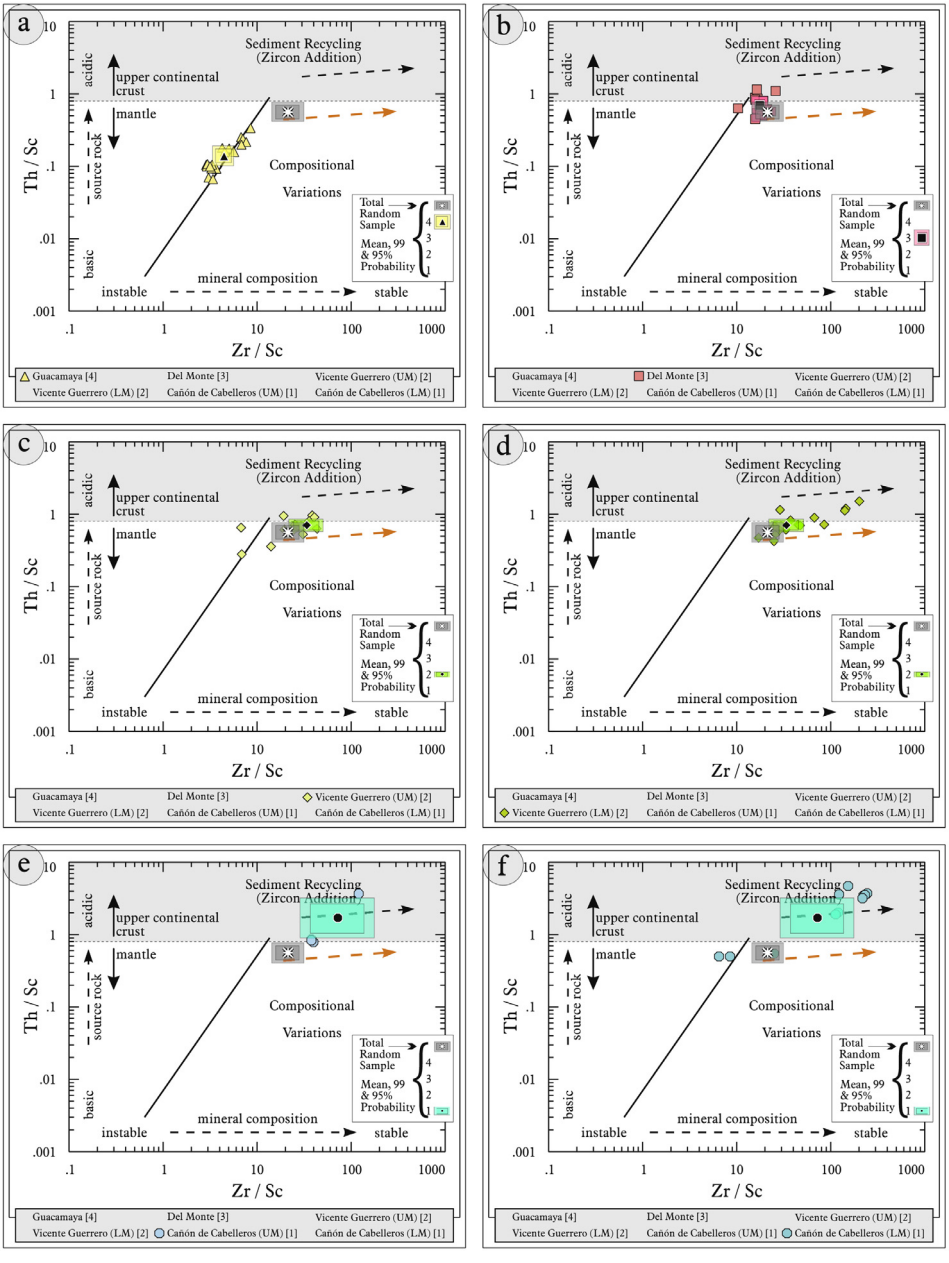

Fig. 19. Geochemical classification of recycling of the Tamatán Group: Zr/Sc–Th/Sc diagram after [14].

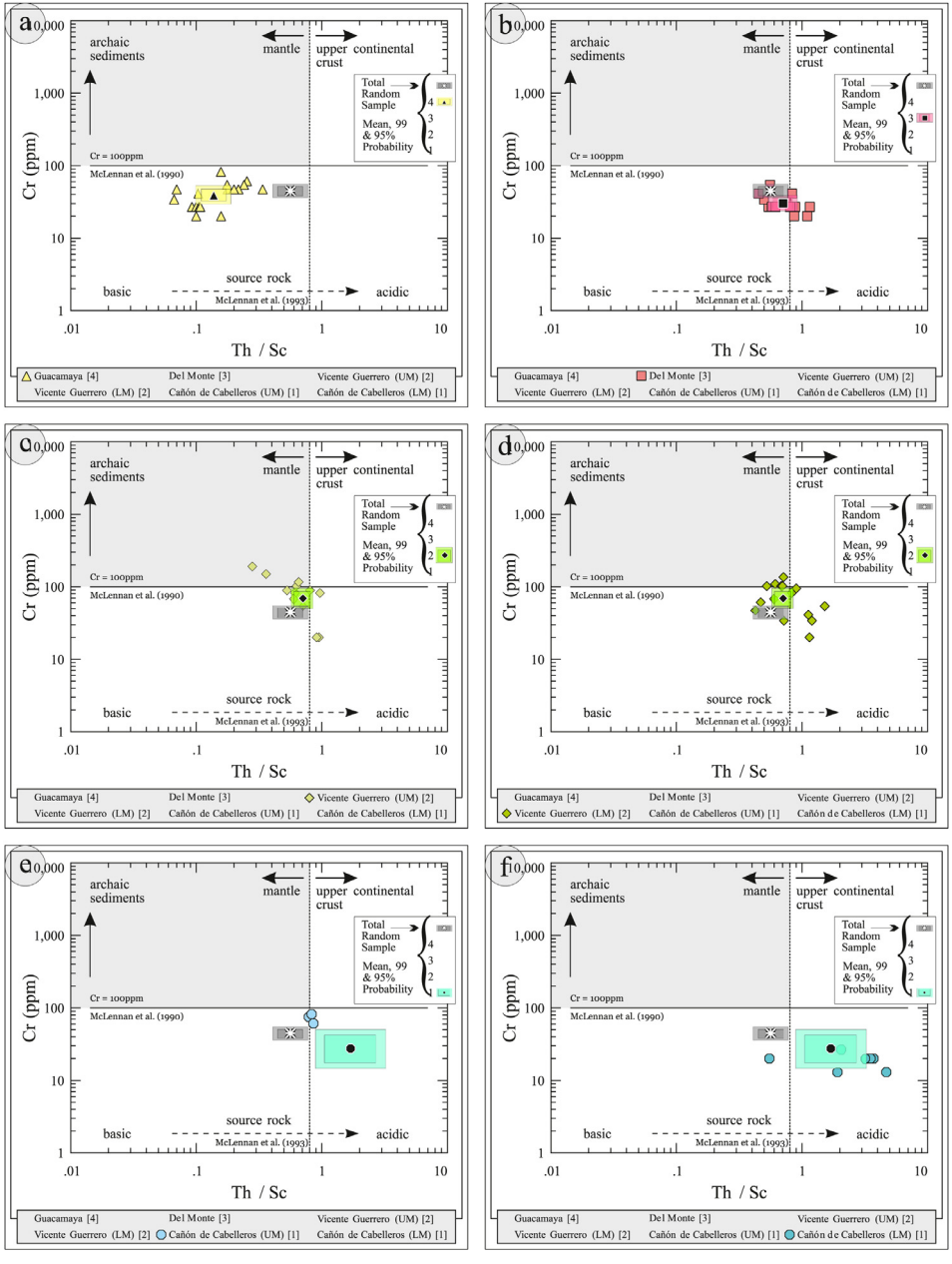

Fig. 20. Geochemical classification of the source area and geotectonic environment of the Tamatán Group: Th/Sc–Cr diagram after [10].

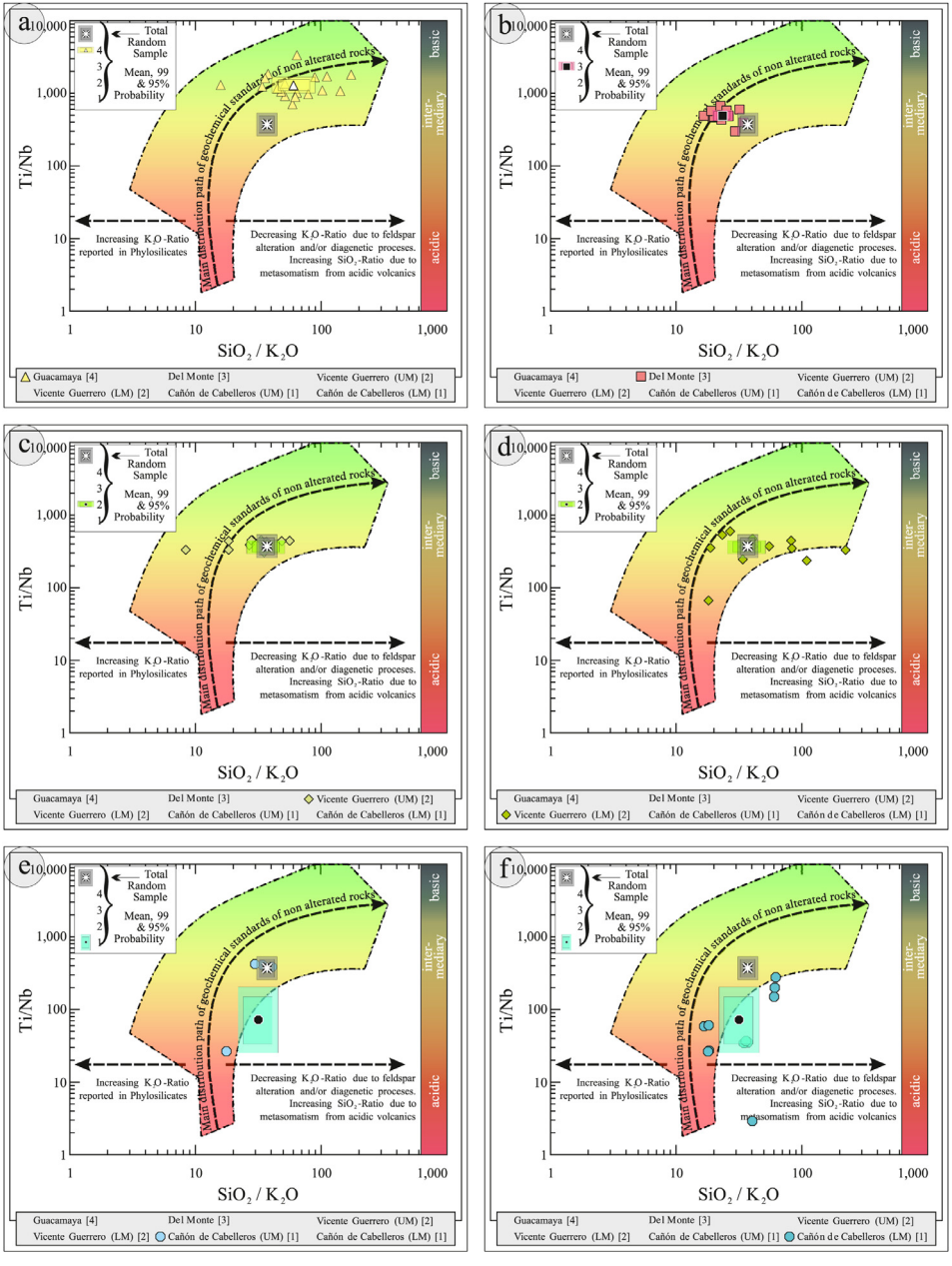

Fig. 21. Geochemical classification of the source area of the Tamatán Group: SiO_2/K_2O–Ti/Nb diagram after [10].

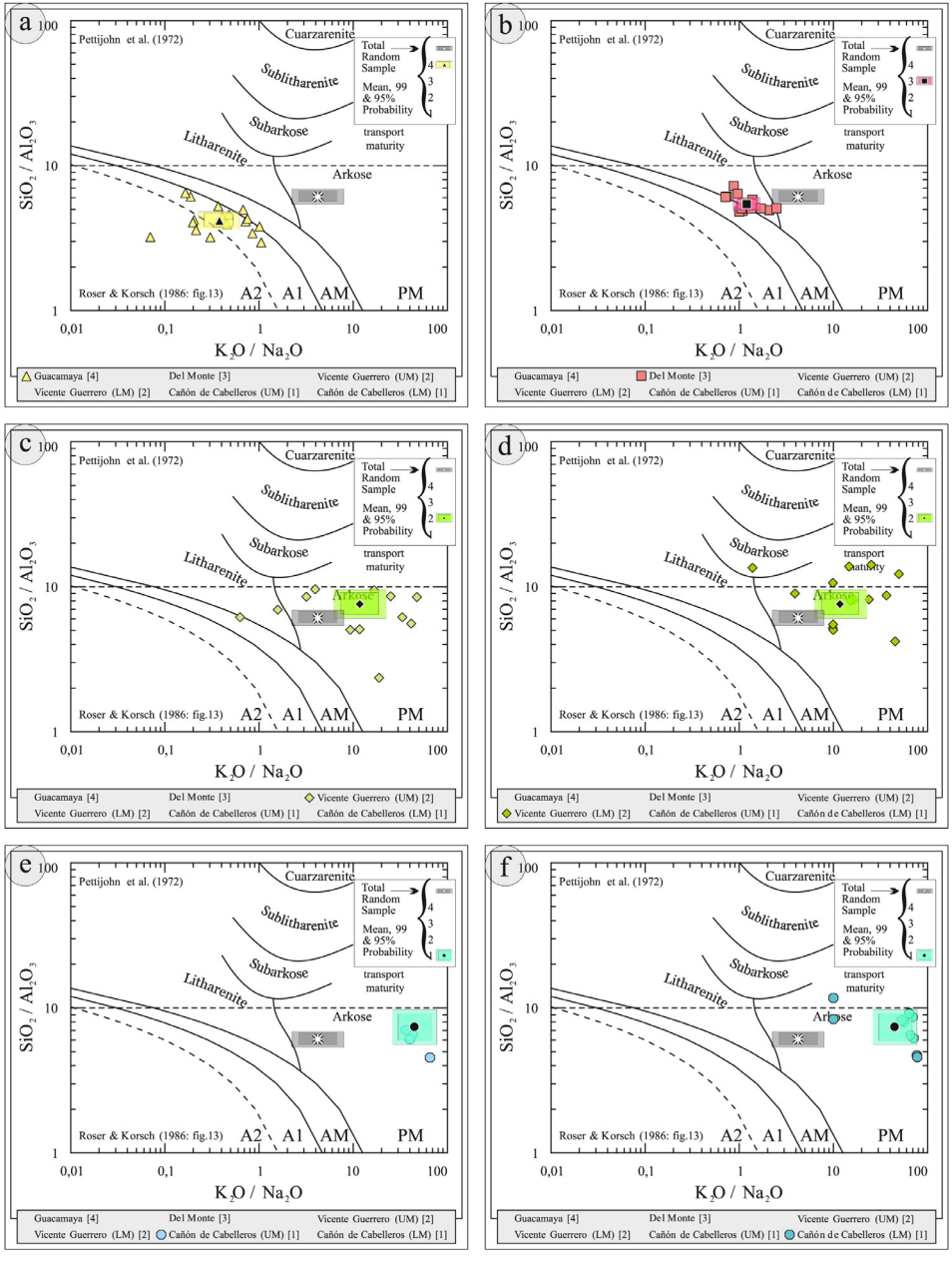

Fig. 22. Geochemical sediment classification and classification of the geotectonic environment of the Tamatán Group: K_2O/Na_2O–SiO_2/Al_2O_3 diagram after [10].

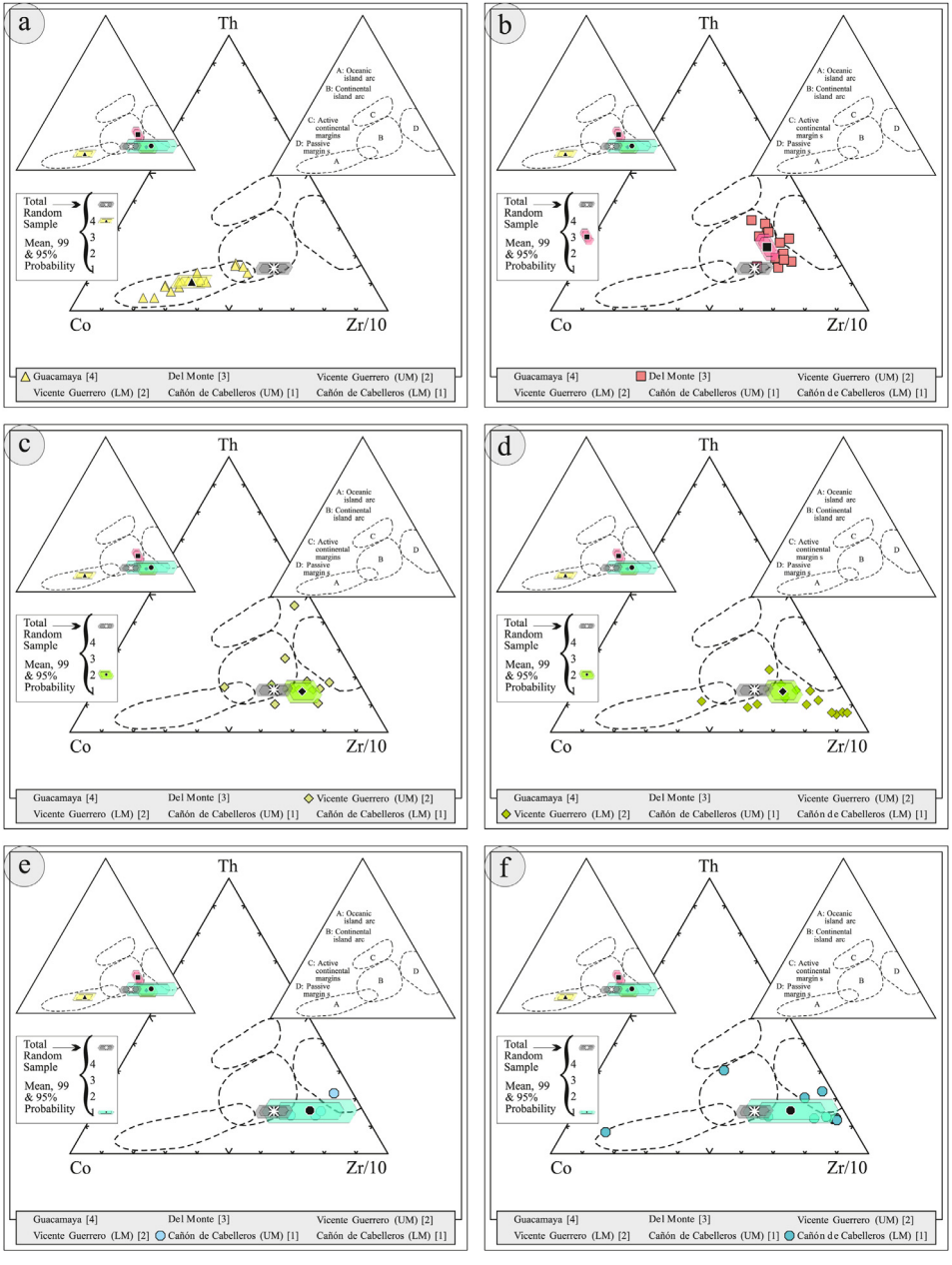

Fig. 23. Geochemical classification of the source area and geotectonic environment of the Tamatán Group: Th–Co–Zr/10 diagram after [15].

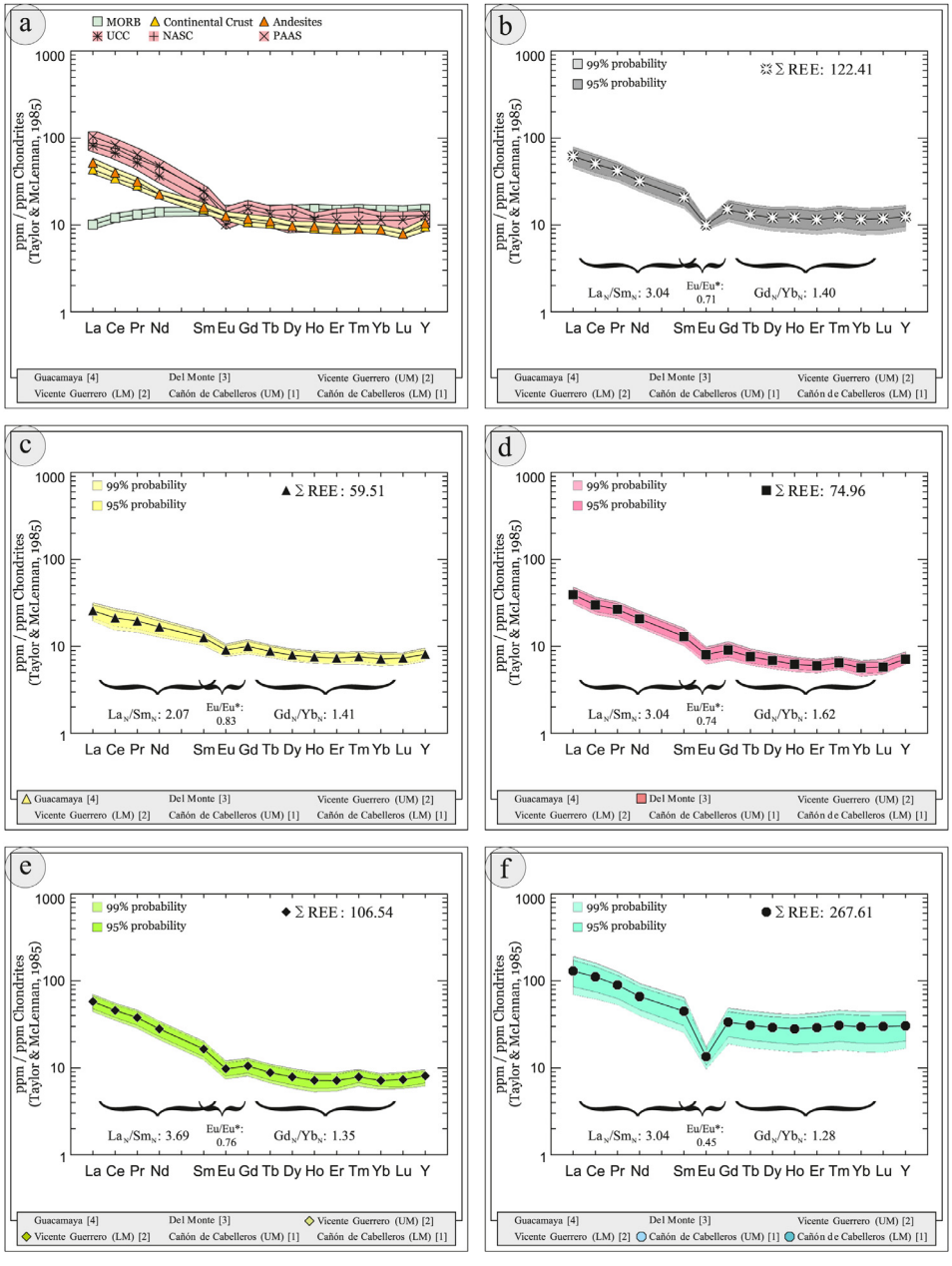

Fig. 24. REE pattern of the Tamatán Group after [16].

4.4. U-Th-Pb data of detrital zircons

Tables 14-21.

Table 14
LA-MC-ICPMS U-Th-Pb data of detrital zircons from the Cañón de Caballeros Formation: Sample CC64–04, Caballeros Canyon, Huizachal-Peregrina Anticlinorium, Tamaulipas, México; Coordinates: R 14–470,240 E, 2,631,770 N.

Sample: CC64-04 Spot (1)	Analysis	U [ppm]a	Pb [ppm]a	Th [ppm]a	$^{206}Pb/^{204}Pb$	Th/U[a]	U/Th	Ratio (2)								Aparente age [Ma]						Conc. %
								$^{207}Pb/^{235}U$[b]	2 σ[d]	$^{208}Pb/^{238}U$[b]	2 σ[d]	rho[c]	$^{207}Pb/^{206}Pb$[e]	2 σ[d]		$^{207}Pb/^{235}U$	2 σ	$^{206}Pb/^{238}U$ (3)	2 σ	$^{207}Pb/^{206}Pb$ (3)	2 σ	
020	A_166	103	32	59	211702	0.57	1.75	4.416	0.148	0.30540	0.00752	0.74	0.10487	0.00238		1715	57	1718	42	**1712**	**42**	100
021	A_167	116	9	76	57251	0.66	1.52	0.569	0.046	0.07355	0.00226	0.38	0.05611	0.00422		457	37	**458**	**14**	456	162	100
022	A_168	95	19	37	699	0.39	2.57	2.234	0.080	0.20273	0.00504	0.69	0.07992	0.00208		1192	43	1190	30	**1195**	**51**	100
030	A_178	67	18	37	121660	0.55	1.83	3.335	0.173	0.26927	0.00750	0.54	0.08982	0.00392		1489	77	1537	43	**1422**	**82**	108
037	A_185	272	59	95	393700	0.35	2.85	2.474	0.082	0.21595	0.00530	0.74	0.08310	0.00186		1265	42	1260	31	**1272**	**43**	99
039	A_187	59	4	38	346	0.64	1.55	0.505	0.026	0.06620	0.00174	0.52	0.05538	0.00240		415	21	**413**	**11**	427	95	97
051	A_201	125	28	32	1939	0.26	3.91	2.646	0.109	0.22402	0.00576	0.63	0.08568	0.00274		1314	54	1303	34	**1331**	**62**	98
060	A_212	175	11	93	74394	0.53	1.88	0.482	0.025	0.06352	0.00168	0.51	0.05508	0.00246		400	21	**397**	**11**	416	97	96
067	A_219	248	42	55	281149	0.22	4.52	1.693	0.057	0.16901	0.00416	0.73	0.07264	0.00168		1006	34	1007	25	**1004**	**47**	100
068	A_220	74	5	61	320	0.83	1.21	0.536	0.053	0.06876	0.00234	0.34	0.05658	0.00524		436	43	**429**	**15**	474	200	90
073	A_227	174	12	110	78368	0.64	1.57	0.511	0.020	0.06732	0.00168	0.64	0.05503	0.00166		419	16	**420**	**10**	413	66	102
075	A_229	112	8	101	54013	0.90	1.12	0.554	0.025	0.07189	0.00184	0.57	0.05589	0.00208		448	20	**448**	**11**	448	81	100
077	A_231	137	10	68	65047	0.50	2.01	0.544	0.027	0.07076	0.00184	0.53	0.05572	0.00230		441	22	**441**	**11**	441	90	100
081	A_235	256	20	85	133531	0.33	2.99	0.600	0.044	0.07809	0.00230	0.41	0.05572	0.00370		477	35	**485**	**14**	441	144	110
090	A_251	50	8	6	55216	0.12	8.36	1.636	0.071	0.16410	0.00426	0.59	0.07232	0.00254		984	43	980	25	**995**	**71**	98
091	A_252	102	7	70	118	0.69	1.44	0.507	0.022	0.06714	0.00172	0.58	0.05472	0.00198		416	18	**419**	**11**	400	81	105
099	A_262	93	5	91	72	0.98	1.02	0.522	0.036	0.05320	0.00158	0.44	0.07122	0.00436		427	29	334	**10**	**964**	122	35
107	A_270	47	9	18	58664	0.39	2.56	1.978	0.082	0.18731	0.00482	0.62	0.07657	0.00250		1108	46	1107	28	**1110**	**64**	100
109	A_272	69	13	50	537	0.72	1.40	2.138	0.093	0.19269	0.00502	0.60	0.08047	0.00280		1161	50	1136	30	**1209**	**68**	94
110	A_273	77	6	62	41011	0.80	1.24	0.627	0.044	0.08009	0.00234	0.42	0.05679	0.00362		494	35	**497**	**15**	483	139	103

Abreviation: a = U and Pb concentration and Th/U ratios are calculated relative to GJ-1 reference zircon; b = Corrected for background and within -run Pb/U fractionation and normalized to reference zircon GJ-1 (ID-TIMS values/measured value); $^{207}Pb/^{235}U$ calculated using ($^{207}Pb/^{206}Pb$)/($^{238}U/^{206}Pb$*1/137.88); c = *Rho* is the error correlation defined as the quotient of the propagated errors of the $^{206}Pb/^{238}U$ and the $^{207}Pb/^{235}U$ ratio; d = Quadratic addition of within-run errors (2SD) and daily reproducibility of GJ-1 (2SD); e = Corrected for mass-bias by normalizing to GJ-1 reference zircon (~ 0.6 per atomic mass unit) and common Pb using the model Pb composition of Stacey & Kramers (1975). (1) Sample identifier, spot number [*missing numbers*: spots were omitted due to high analytical errors], (2) Isotope ratios corrected for common Pb using measured ^{204}Pb for correction. Individual errors are given as 2-sigma standard deviation; (3) Most reliable apparent ages are in bold letters. Note: If the average of apparent ages is mid-Proterozoic and older (>900 Ma) then $^{207}Pb/^{206}Pb$ ages are considered as most reliable apparent ages; for younger values $^{206}Pb/^{238}U$ ages are used.

Table 15
CL-images and best ages from selected zircons of the Cañón de Caballeros Formation (Silurian).

Cañón de Caballeros Formation (Silurian)			
			
CC64-04–020 → 1712±42 Ma	CC64-04–030 → 1422±82 Ma	CC64-04–051 → 1331±62 Ma	CC64-04–037 → 1272±43 Ma
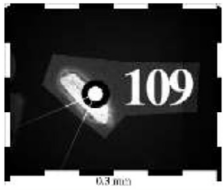	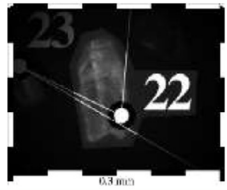		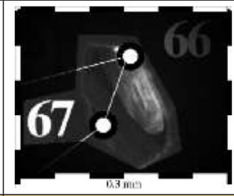
CC64-04–109 → 1209±68 Ma	CC64-04–022 → 1195±51 Ma	CC64-04–107 → 1110±64 Ma	CC64-04–067 → 1004±57 Ma
		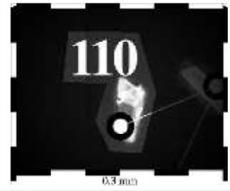	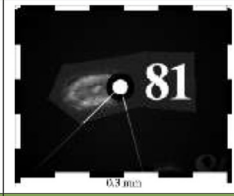
CC64-04–090 → 995±71 Ma	CC64-04–099 → 964±122 Ma	CC64-04–110 → 497±15 Ma	CC64-04–081 → 485±14 Ma
		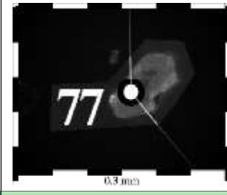	
CC64-04–021 → 458±14 Ma	CC64-04–075 → 448±11 Ma	CC64-04–077 → 441±11 Ma	CC64-04–068 → 429±15 Ma
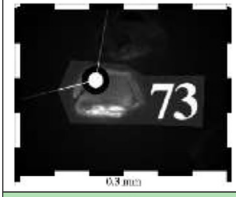	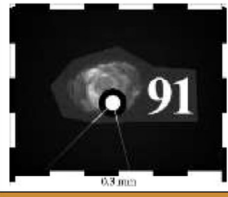		
CC64-04–073 → 420±10 Ma	CC64-04–091 → 419±11 Ma	CC64-04–039 → 413±11 Ma	CC64-04–060 → 397±11 Ma

Table 16
LA-MC-ICPMS U-Th-Pb data of selected detrital zircons from the Vicente Guerrero Formation: Sample CC54–14, Caballeros Canyon, Huizachal-Peregrina Anticlinorium, Tamaulipas, México; Coordinates: R 14–4,697,720 E, 2,632,328 N.

Sample: CC5414 Spot (1)	Analysis	U [ppm]a	Pb [ppm]a	Th [ppm]a	$^{206}Pb/^{204}Pb$	Th/U[a]	U/Th	Ratio (2)							Aparente age [Ma]						Conc. %
								$^{207}Pb/^{235}U^{b}$	2 σ[d]	$^{208}Pb/^{232}U^{b}$	2 σ[d]	rho[c]	$^{207}Pb/^{206}Pb^{e}$	2 σ[d]	$^{207}Pb/^{235}U$	2 σ	$^{206}Pb/^{238}U$ (3)	2 σ	$^{207}Pb/^{206}Pb$ (3)	2 σ	
009	14-009	125	23	61	7626	0.49	2.05	2.03	0.07	0.183	0.005	0.74	0.080	0.002	1125	39	1082	28	**1209**	**46**	90
012	14-012	387	96	14	673682	0.04	27.45	3.12	0.10	0.249	0.006	0.77	0.091	0.002	1437	48	1433	37	**1443**	**40**	99
015	14-015	52	12	24	81931	0.46	2.15	2.64	0.13	0.226	0.006	0.57	0.085	0.003	1312	64	1314	37	**1309**	**77**	100
018	14-018	32	9	9	63741	0.27	3.68	3.92	0.14	0.286	0.008	0.71	0.099	0.003	1617	60	1623	43	**1610**	**48**	101
019	14-019	45	13	16	89283	0.34	2.90	3.88	0.17	0.283	0.008	0.62	0.100	0.004	1610	72	1604	44	**1617**	**66**	99
026	14-026	69	13	33	92351	0.47	2.12	2.06	0.08	0.192	0.005	0.70	0.078	0.002	1136	43	1130	29	**1147**	**53**	99
030	14-030	180	12	68	520	0.38	2.65	0.59	0.02	0.069	0.002	0.62	0.062	0.002	468	20	**428**	**11**	669	71	64
031	14-031	75	11	15	182	0.20	4 94	1.46	0.06	0.153	0.004	0.62	0.069	0.002	913	39	920	25	**895**	**70**	103
038	14-038	20	4	5	25531	0.26	3.92	1.89	0.12	0.185	0.006	0.47	0.074	0.004	1078	70	1092	33	**1051**	**116**	104
041	14-041	87	13	41	91261	0.48	2.09	1.51	0.06	0.150	0.004	0.65	0.073	0.002	933	38	904	24	**1003**	**62**	90
042	14-042	95	22	18	155568	0.19	5.40	2.82	0.11	0.233	0.006	0.69	0.088	0.002	1360	52	1351	35	**1375**	**53**	98
071	14-071	55	3	15	18532	0.28	3.59	0.40	0.02	0.048	0.001	0.49	0.059	0.003	338	19	**305**	**8**	575	107	53
073	14-073	170	35	68	1573	0.40	2.50	2.37	0.08	0.209	0.005	0.75	0.082	0.002	1234	42	1224	31	**1251**	**44**	98
074	14-074	132	37	51	1993	0.38	2.61	3.77	0.13	0.281	0.007	0.73	0.097	0.002	1587	56	1595	41	**1576**	**45**	101
079	14-079	524	86	79	604495	0.15	6.60	1.63	0.05	0.164	0.004	0.76	0.072	0.002	981	33	980	25	**981**	**44**	100
080	14-080	165	31	36	25151	0.22	4.64	1.92	0.07	0.185	0.005	0.73	0.076	0.002	1090	38	1093	28	**1083**	**48**	101
091	14-091	259	13	58	88995	0.23	4.43	0.36	0.01	0.049	0.001	0.66	0.053	0.002	309	12	**308**	**8**	317	66	97
101	14-102	296	49	160	347011	0.54	1.85	1.66	0.06	0.167	0.004	0.74	0.072	0.002	995	34	994	25	**998**	**47**	100
103	14-104	39	6	29	493	0.74	1.36	1.52	0.06	0.157	0.004	0.63	0.070	0.002	938	39	938	25	**938**	**67**	100
111	14-111	118	35	49	3392	0.42	2.40	4.25	0.15	0.298	0.008	0.74	0.103	0.002	1684	58	1680	43	**1687**	**42**	100
113	14-113	128	26	31	183585	0.24	4.15	2.24	0.08	0.203	0.005	0.71	0.080	0.002	1194	44	1193	31	**1196**	**51**	100

Abreviation: a = U and Pb concentration and Th/U ratios are calculated relative to GJ-1 reference zircon; b = Corrected for background and within -run Pb/U fractionation and normalized to reference zircon GJ-1 (ID-TIMS values/measured value); $^{207}Pb/^{235}U$ calculated using ($^{207}Pb/^{206}Pb$)/($^{238}U/^{206}Pb$*1/137.88); c = *Rho* is the error correlation defined as the quotient of the propagated errors of the $^{206}Pb/^{238}U$ and the $^{207}Pb/^{235}U$ ratio; d = Quadratic addition of within-run errors (2SD) and daily reproducibility of GJ-1 (2SD); e = Corrected for mass-bias by normalizing to GJ-1 reference zircon (~ 0.6 per atomic mass unit) and common Pb using the model Pb composition of Stacey & Kramers (1975). (1) Sample identifier, spot number [*missing numbers*: spots were omitted due to high analytical errors], (2) Isotope ratios corrected for common Pb using measured ^{204}Pb for correction. Individual errors are given as 2-sigma standard deviation; (3) Most reliable apparent ages are in bold letters. Note: If the average of apparent ages is mid-Proterozoic and older (>900 Ma) then $^{207}Pb/^{206}Pb$ ages are considered as most reliable apparent ages; for younger values $^{206}Pb/^{238}U$ ages are used.

Table 17
CL-images and best ages from zircons of the Vicente Guerrero Formation (Mississippian).

Vicente Guerrero Formation (Mississippian)			
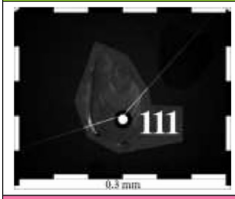	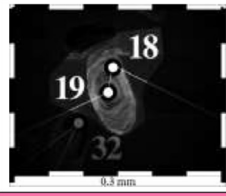		
CC54-14–111 → 1687±42 Ma	CC54-14–018 → 1610±48 Ma	CC54-14–074 → 1576±45 Ma	CC54-14–012 → 1443±40 Ma
	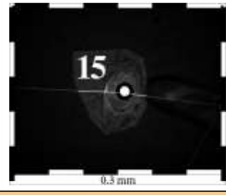	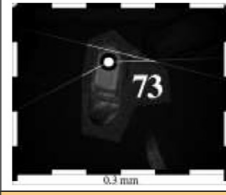	
CC54-14–042 → 1375±53 Ma	CC54-14–015 → 1309±77 Ma	CC54-14–073 → 1251±44 Ma	CC54-14–009 → 1209±46 Ma
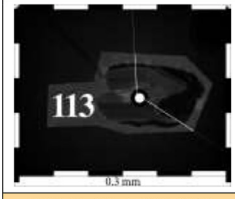	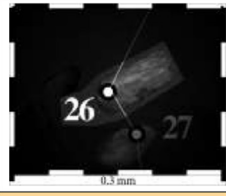	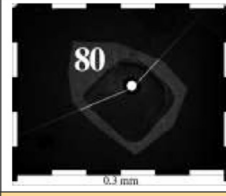	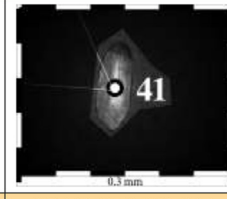
CC54-14–113 → 1196±51 Ma	CC54-14–026 → 1147±53 Ma	CC54-14–080 → 1083±48 Ma	CC54-14–041 → 1003±62 Ma
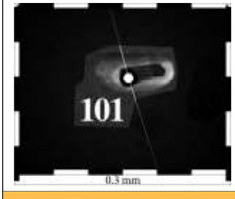	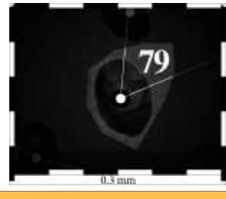		
CC54-14–101 → 998±47 Ma	CC54-14–079 → 981±44 Ma	CC54-14–028 → 950±50 Ma	CC54-14–103 → 938±67 Ma
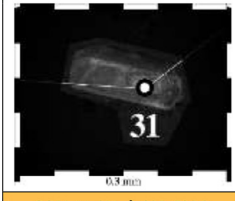			
CC54-14–031 → 895±70 Ma	CC54-14–030 → 428±11 Ma	CC54-14–091 → 419±08 Ma	CC54-14–071 → 305±08 Ma

Table 18
LA-MC-ICPMS U-Th-Pb data of detrital zircons from the Del Monte Formation: Sample CC207–07, Peregrina Canyon, Huizachal-Peregrina Anticlinorium, Tamaulipas, México; Coordinates: R 14–473,181 E, 2,629,063 N.

Sample: CP207-07 Spot (1)	Analysis	U [ppm]a	Pb [ppm]a	Th [ppm]a	$^{206}Pb/^{204}Pb$	Th/U[a]	U/Th	Ratio (2)								Aparente age [Ma]						Conc. %
								$^{207}Pb/^{235}U^b$	2 σ^d	$^{206}Pb/^{238}U^b$	2 σ^d	*rho*[c]	$^{207}Pb/^{206}Pb^*$	2 σ^d		$^{207}Pb/^{235}U$	2 σ	$^{206}Pb/^{238}U$ (3)	2 σ	$^{207}Pb/^{206}Pb$ (3)	2 σ	
001	A_004	793	110	94	22927	0.12	8.48	1.457	0.048	0.13894	0.00348	0.77	0.07608	0.00160		913	30	**839**	**21**	1097	42	76
008	A_011	323	74	27	503452	0.08	12.15	2.676	0.088	0.22768	0.00568	0.76	0.08523	0.00182		1322	43	1322	33	**1321**	**41**	100
010	A_013	109	18	16	364	0.14	6.91	1.671	0.060	0.16690	0.00422	0.71	0.07260	0.00184		997	36	995	25	**1003**	**51**	99
012	A_015	128	57	28	392291	0.22	4.57	9.549	0.314	0.44903	0.01124	0.76	0.15424	0.00328		2392	79	2391	60	**2394**	**36**	100
014	A_017	152	36	38	249101	0.25	3.97	2.883	0.097	0.23955	0.00600	0.74	0.08729	0.00198		1377	47	1384	35	**1367**	**43**	101
027	A_039	780	135	181	6668	0.23	4.30	2.020	0.066	0.17350	0.00430	0.76	0.08446	0.00178		1122	37	1031	26	**1303**	**41**	79
028	A_040	256	56	67	191717	0.26	3.80	2.496	0.083	0.21749	0.00542	0.75	0.08324	0.00184		1271	42	1269	32	**1275**	**43**	100
029	A_041	172	34	24	1243	0.14	7.20	2.155	0.074	0.19562	0.00488	0.73	0.07991	0.00186		1167	40	1152	29	**1195**	**46**	96
037	A_049	119	30	31	206067	0.26	3.82	3.129	0.111	0.25014	0.00630	0.71	0.09071	0.00226		1440	51	1439	36	**1440**	**47**	100
049	A_063	91	8	45	146	0.49	2.03	1.134	0.044	0.09322	0.00238	0.66	0.08819	0.00256		769	30	**575**	**15**	1387	55	41
064	A_080	398	74	142	2959	0.36	2.81	1.976	0.066	0.18597	0.00458	0.74	0.07706	0.00172		1107	37	1100	27	**1123**	**44**	98
078	A_101	415	59	215	413387	0.52	1.93	1.514	0.050	0.14262	0.00350	0.74	0.07701	0.00172		936	31	**860**	**21**	1121	44	77
080	A_103	2131	142	326	1859	0.15	6.54	0.688	0.025	0.06679	0.00166	0.69	0.07470	0.00194		532	19	**417**	**10**	1060	52	39
086	A_111	369	61	107	2072	0.29	3.43	1.645	0.055	0.16569	0.00406	0.74	0.07202	0.00162		988	33	988	24	**987**	**46**	100
087	A_112	529	91	101	635183	0.19	5.22	1.764	0.058	0.17175	0.00420	0.74	0.07448	0.00166		1032	34	1022	25	**1054**	**45**	97
090	A_115	428	83	163	583465	0.38	2.63	2.110	0.070	0.19492	0.00476	0.74	0.07850	0.00174		1152	38	1148	28	**1160**	**44**	99
096	A_123	70	16	21	109904	0.30	3.35	2.639	0.106	0.22373	0.00570	0.64	0.08554	0.00264		1312	52	1302	33	**1328**	**59**	98
100	A_127	899	96	219	10114	0.24	4.10	1.145	0.038	0.10716	0.00262	0.74	0.07751	0.00172		775	26	**656**	**16**	1134	44	58
104	A_131	174	36	49	252727	0.28	3.57	2.304	0.079	0.20634	0.00506	0.72	0.08098	0.00192		1213	41	1209	30	**1221**	**46**	99
110	A_137	72	19	45	1557	0.63	1.60	3.306	0.117	0.25847	0.00640	0.70	0.09277	0.00234		1483	52	1482	37	**1483**	**48**	100

Abreviation: a = U and Pb concentration and Th/U ratios are calculated relative to GJ-1 reference zircon; b = Corrected for background and within -run Pb/U fractionation and normalized to reference zircon GJ-1 (ID-TIMS values/measured value); $^{207}Pb/^{235}U$ calculated using ($^{207}Pb/^{206}Pb$)/($^{238}U/^{206}Pb$*1/137.88); c = *Rho* is the error correlation defined as the quotient of the propagated errors of the $^{206}Pb/^{238}U$ and the $^{207}Pb/^{235}U$ ratio; d = Quadratic addition of within-run errors (2SD) and daily reproducibility of GJ-1 (2SD); e = Corrected for mass-bias by normalizing to GJ-1 reference zircon (~ 0.6 per atomic mass unit) and common Pb using the model Pb composition of Stacey & Kramers (1975). (1) Sample identifier, spot number [*missing numbers*: spots were omitted due to high analytical errors], (2) Isotope ratios corrected for common Pb using measured ^{204}Pb for correction. Individual errors are given as 2-sigma standard deviation; (3) Most reliable apparent ages are in bold letters. Note: If the average of apparent ages is mid-Proterozoic and older (>900 Ma) then $^{207}Pb/^{206}Pb$ ages are considered as most reliable apparent ages; for younger values $^{206}Pb/^{238}U$ ages are used.

Table 19
CL-images and best ages from zircons of the Del Monte Formation (Pennsylvanian).

Del Monte Formation (Pennsylvanian)			
			
CP207-07–012 → 2394±36 Ma	CP207-07–110 → 1483±48 Ma	CP207-07–037 → 1440±47 Ma	CP207-07–014 → 1367±43 Ma
			
CP207-07–096 → 1328±59 Ma	CP207-07–027 → 1303±41 Ma	CP207-07–028 → 1275±43 Ma	CP207-07–104 → 1221±46 Ma
	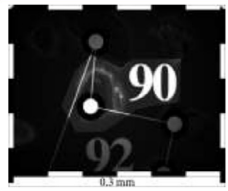		
CP207-07–029 → 1195±46 Ma	CP207-07–090 → 1160±44 Ma	CP207-07–064 → 1123±44 Ma	CP207-07–001 → 1097±42 Ma
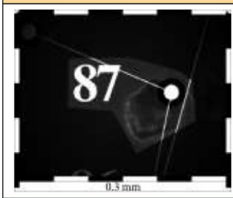			
CP207-07–087 → 1054±45 Ma	CP207-07–010 → 1003±51 Ma	CP207-07–086 → 987±46 Ma	CP207-07–078 → 860±21 Ma
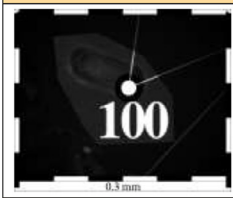			
CP207-07–100 → 656±16 Ma	CP207-07–007 → 0586±15 Ma	CP207-07–049 → 575±15 Ma	CP207-07–080 → 417±10 Ma

Table 20
LA-MC-ICPMS U-Th-Pb data of detrital zircons from the Guacamaya Formation: Sample CC197–03, Peregrina Canyon, Huizachal-Peregrina Anticlinorium, Tamaulipas, México; Coordinates: R 14–474,593 E, 2,629,044 N.

Sample: CP197.03 Spot (1)	Analysis	U [ppm]a	Pb [ppm]a	Th [ppm]a	$^{206}Pb/^{204}Pb$	Th/U[a]	U/Th	Ratio (2)								Aparente age [Ma]						Conc. %
								$^{207}Pb/^{235}U^b$	2 σ[d]	$^{208}Pb/^{232}U^b$	2 σ[d]	*rho*[c]	$^{207}Pb/^{206}Pb^e$	2 σ[d]		$^{207}Pb/^{235}U$	2 σ	$^{206}Pb/^{238}U$ (3)	2 σ	$^{207}Pb/^{206}Pb$ (3)	2 σ	
001	03-001	69	4	17	24031	0.25	4.01	0.376	0.021	0.0517	0.0014	0.50	0.053	0.003		324	18	**325**	9	319	109	102
002	03-002	59	3	9	19443	0.16	6.26	0.358	0.023	0.0491	0.0014	0.45	0.053	0.003		310	20	**309**	9	322	129	96
004	03-004	53	3	11	212	0.21	4.79	0.351	0.020	0.0488	0.0014	0.48	0.052	0.003		306	18	**307**	9	297	116	103
005	03-005	37	2	7	58	0.19	5.21	0.351	0.054	0.0477	0.0021	0.29	0.053	0.008		306	47	**301**	13	344	333	87
006	03-006	31	1	6	9861	0.20	4.94	0.341	0.025	0.0476	0.0014	0.40	0.052	0.004		298	22	**300**	9	284	157	105
012	03-012	251	29	54	196897	0.21	4.66	1.113	0.039	0.1163	0.0030	0.74	0.069	0.002		760	27	**709**	18	912	48	78
013	03-013	138	7	38	46455	0.28	3.58	0.360	0.016	0.0501	0.0013	0.62	0.052	0.002		312	13	**315**	8	292	77	108
014	03-014	95	4	25	187	0.27	3.77	0.340	0.022	0.0464	0.0014	0.44	0.053	0.003		297	20	**293**	9	331	134	89
018	03-018	71	3	25	149	0.36	2.80	0.347	0.025	0.0480	0.0014	0.42	0.052	0.003		302	22	**302**	9	303	149	100
019	03-019	68	3	19	22263	0.28	3.62	0.353	0.019	0.0489	0.0013	0.52	0.052	0.002		307	16	**308**	8	301	103	102
020	03-020	52	3	11	17247	0.21	4.74	0.361	0.024	0.0496	0.0014	0.44	0.053	0.003		313	21	**312**	9	320	134	97
031	03-031	19	1	4	6573	0.21	4.81	0.375	0.074	0.0516	0.0027	0.27	0.053	0.010		323	64	**324**	17	314	433	103
032	03-032	27	1	6	8969	0.23	4.29	0.365	0.061	0.0498	0.0023	0.28	0.053	0.008		316	52	**313**	15	333	361	94
033	03-033	39	2	11	70	0.27	3.71	0.354	0.036	0.0489	0.0017	0.34	0.052	0.005		308	31	**308**	11	306	215	101
034	03-034	61	3	17	264	0.28	3.57	0.337	0.026	0.0449	0.0014	0.39	0.055	0.004		295	23	**283**	9	394	161	72
036	03-036	74	3	16	481	0.21	4.68	0.322	0.019	0.0449	0.0013	0.48	0.052	0.003		283	16	**283**	8	288	116	98
038	03-038	125	6	21	2101	0.17	5.84	0.328	0.015	0.0448	0.0012	0.57	0.053	0.002		288	14	**282**	8	333	88	85
043	03-043	74	3	19	19122	0.26	3.84	0.320	0.017	0.0383	0.0011	0.52	0.061	0.003		282	15	**242**	7	628	98	39
050	03-050	43	2	9	249	0.20	4.96	0.355	0.022	0.0473	0.0013	0.46	0.054	0.003		308	19	**298**	8	388	124	77
051	03-051	55	3	11	17492	0.20	5.12	0.342	0.019	0.0465	0.0013	0.49	0.053	0.003		299	17	**293**	8	345	112	85
052	03-052	37	2	8	613	0.21	4.85	0.363	0.024	0.0471	0.0014	0.44	0.056	0.003		314	21	**297**	9	446	131	67
053	03-053	62	3	17	19553	0.27	3.66	0.360	0.020	0.0464	0.0013	0.51	0.056	0.003		312	17	**292**	8	464	104	63
064	03-064	37	2	8	11754	0.21	4.68	0.387	0.025	0.0470	0.0014	0.45	0.060	0.004		332	22	**296**	9	591	127	50
065	03-065	37	2	8	12038	0.21	4.84	0.347	0.027	0.0479	0.0015	0.40	0.053	0.004		303	23	**302**	9	312	160	97
068	03-068	151	29	35	890	0.23	4.35	2.044	0.077	0.1918	0.0050	0.69	0.077	0.002		1130	43	1131	30	**1129**	**55**	100
075	03-075	61	3	11	252	0.18	5.67	0.389	0.023	0.0533	0.0015	0.47	0.053	0.003		334	20	**335**	9	325	121	103
076	03-076	217	11	45	77648	0.21	4.78	0.384	0.015	0.0526	0.0014	0.66	0.053	0.002		330	13	**330**	9	329	68	100
077	03-077	84	16	36	1050	0.43	2.31	2.044	0.075	0.1908	0.0050	0.71	0.078	0.002		1130	41	1126	29	**1140**	**51**	99
081	03-081	74	4	13	133	0.18	5.52	0.370	0.020	0.0507	0.0014	0.51	0.053	0.002		320	17	**319**	9	328	105	97
082	03-082	63	3	13	54	0.20	4.90	0.370	0.028	0.0507	0.0015	0.40	0.053	0.004		320	25	**319**	10	326	160	98
098	03-098	51	2	10	16168	0.20	4.96	0.336	0.024	0.0468	0.0014	0.41	0.052	0.003		294	21	**295**	9	292	151	101
099	03-099	35	2	6	11544	0.18	5.50	0.349	0.028	0.0481	0.0015	0.38	0.053	0.004		304	24	**303**	9	312	169	97
100	03-100	83	4	30	27503	0.37	2.71	0.353	0.020	0.0487	0.0014	0.49	0.053	0.003		307	17	**307**	9	307	113	100
101	03-101	89	4	20	234	0.22	4.55	0.332	0.026	0.0462	0.0014	0.39	0.052	0.004		291	23	**291**	9	294	165	99
102	03-102	35	2	8	114	0.22	4.52	0.341	0.029	0.0466	0.0015	0.37	0.053	0.004		298	25	**294**	9	333	178	88
105	03-105	67	3	12	2173	0.18	5.41	0.322	0.039	0.0450	0.0017	0.31	0.052	0.006		284	34	**284**	11	282	260	101
106	03-106	53	2	9	16120	0.18	5.60	0.323	0.026	0.0443	0.0014	0.38	0.053	0.004		285	23	**279**	9	328	169	85
110	03-110	53	3	11	112	0.22	4.60	0.376	0.023	0.0517	0.0015	0.46	0.053	0.003		324	20	**325**	9	322	124	101
111	03-111	54	3	10	17198	0.19	5.32	0.337	0.021	0.0467	0.0013	0.46	0.052	0.003		295	18	**294**	8	301	125	98

Abreviation: a = U and Pb concentration and Th/U ratios are calculated relative to GJ-1 reference zircon; b = Corrected for background and within -run Pb/U fractionation and normalized to reference zircon GJ-1 (ID-TIMS values/measured value); $^{207}Pb/^{235}U$ calculated using ($^{207}Pb/^{206}Pb$)/($^{238}U/^{206}Pb$*1/137.88); c = *Rho* is the error correlation defined as the quotient of the propagated errors of the $^{206}Pb/^{238}U$ and the $^{207}Pb/^{235}U$ ratio; d = Quadratic addition of within-run errors (2SD) and daily reproducibility of GJ-1 (2SD); e = Corrected for mass-bias by normalizing to GJ-1 reference zircon (~ 0.6 per atomic mass unit) and common Pb using the model Pb composition of Stacey & Kramers (1975). (1) Sample identifier, spot number [*missing numbers*: spots were omitted due to high analytical errors], (2) Isotope ratios corrected for common Pb using measured ^{204}Pb for correction. Individual errors are given as 2-sigma standard deviation; (3) Most reliable apparent ages are in bold letters. Note: If the average of apparent ages is mid-Proterozoic and older (>900 Ma) then $^{207}Pb/^{206}Pb$ ages are considered as most reliable apparent ages; for younger values $^{206}Pb/^{238}U$ ages are used.

Table 21
CL-images and best ages from zircons of the Guacamaya Formation (Permian).

Guacamaya Formation (Permian)			
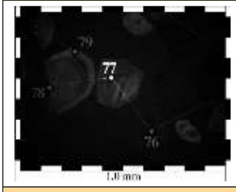			
CP197-03–077 → 1140±51 Ma	CP197-03–068 → 1129±55 Ma	CP197-03–012 → 709±18 Ma	CP197-03–075 → 335±09 Ma
		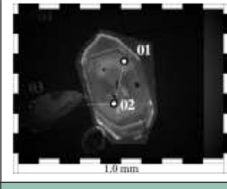	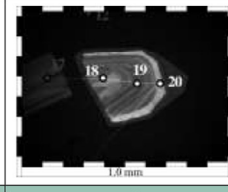
CP197-03–076 → 330±09 Ma	CP197-03–081 → 319±09 Ma	CP197-03–002 → 309±09 Ma	CP197-03–018 → 302±09 Ma
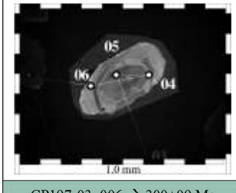	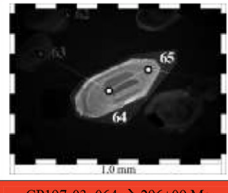		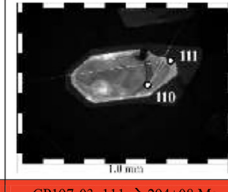
CP197-03–006 → 300±09 Ma	CP197-03–064 → 296±09 Ma	CP197-03–098 → 295±09 Ma	CP197-03–111 → 294±08 Ma
	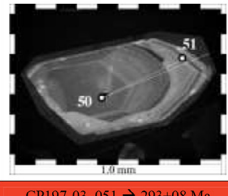	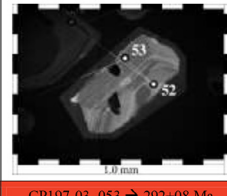	
CP197-03–014 → 293±09 Ma	CP197-03–051 → 293±08 Ma	CP197-03–053 → 292±08 Ma	CP197-03–101 → 291±09 Ma
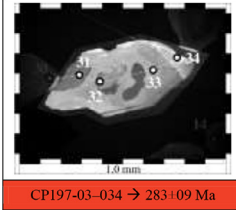	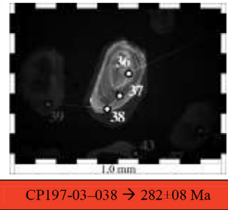	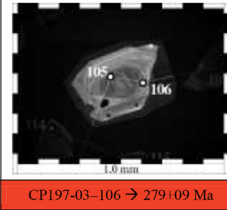	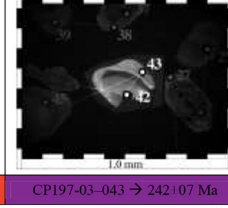
CP197-03–034 → 283±09 Ma	CP197-03–038 → 282±08 Ma	CP197-03–106 → 279±09 Ma	CP197-03–043 → 242±07 Ma

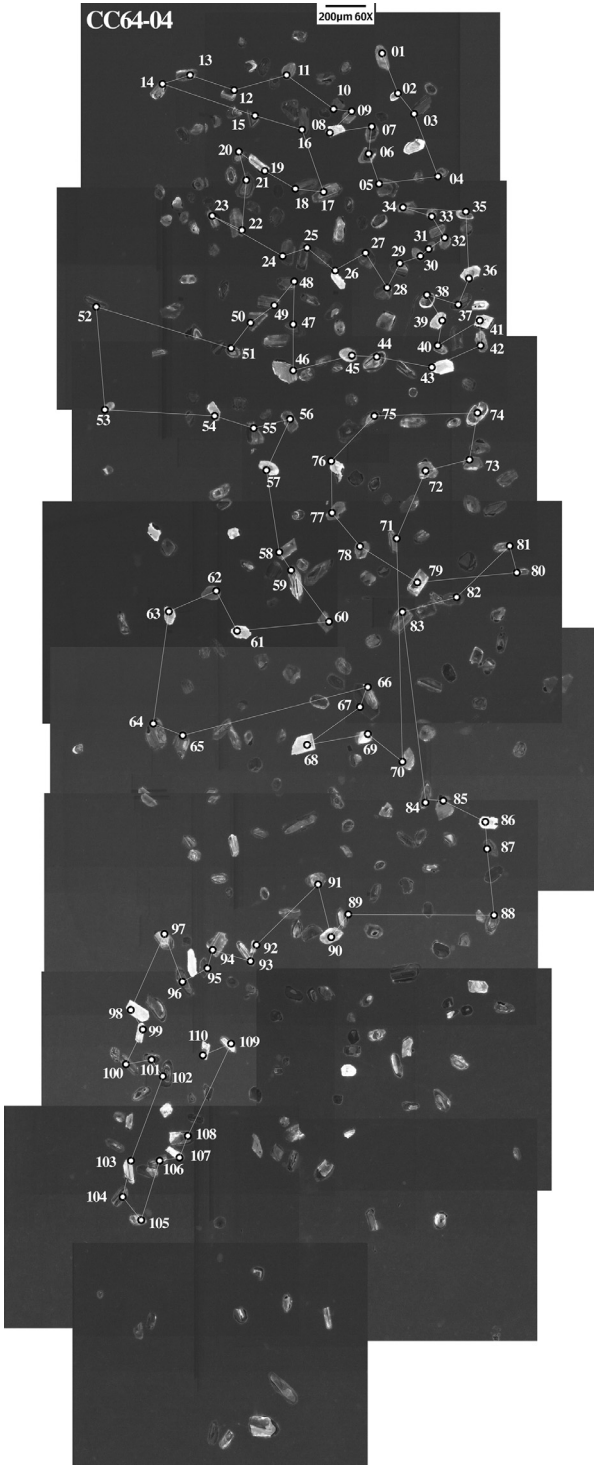

Fig. 25. CL-images of detrital zircons from sample CC64–04: Cañón de Caballeros Formation.

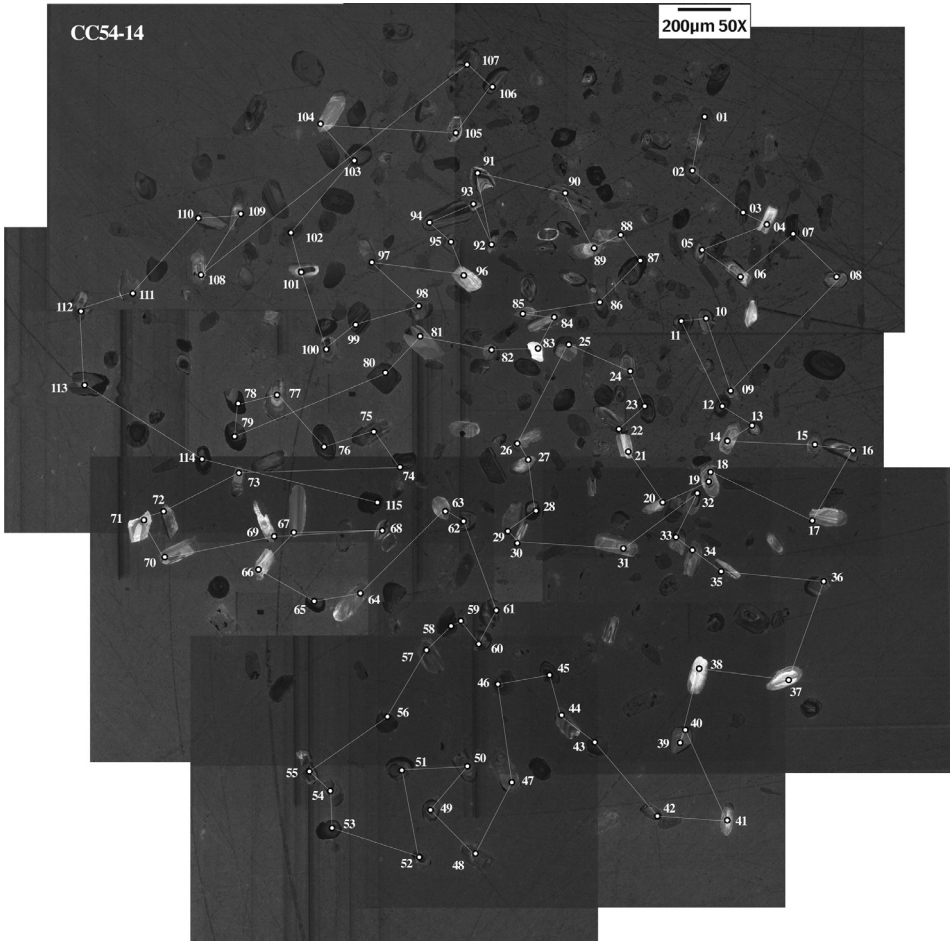

Fig. 26. CL-images of detrital zircons from sample CC54–14: Vicente Guerrero Formation.

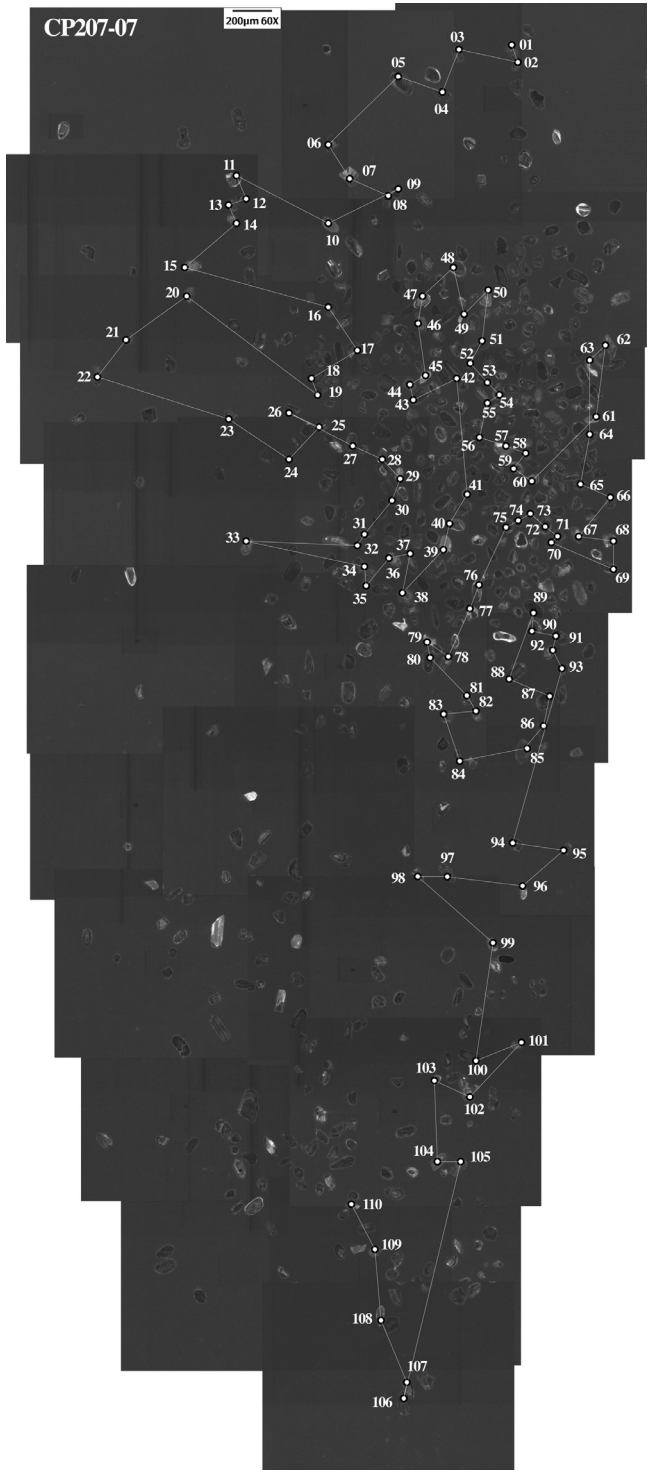

Fig. 27. CL-images of detrital zircons from sample C9207–07: Del Monte Formation.

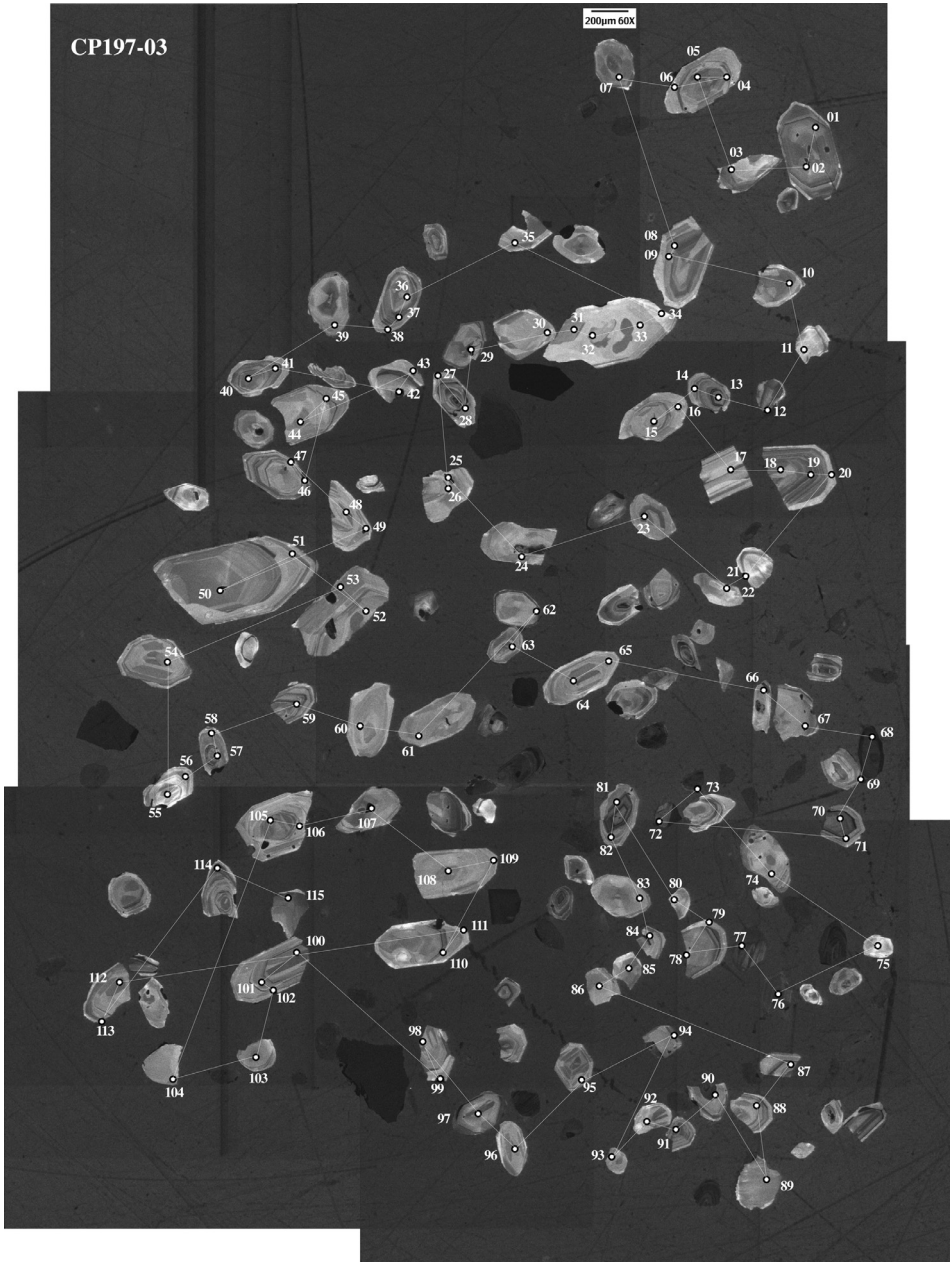

Fig. 28. CL-images of detrital zircons from sample CP197–03: Guacamaya Formation.

Ethics Statement

- This material is the authors' own original work, which has not been previously published elsewhere.
- The paper is not currently being considered for publication elsewhere.
- The paper reflects the authors' own research and analysis in a truthful and complete manner.
- The paper properly credits the meaningful contributions of co-authors and co-researchers.
- The results are appropriately placed in the context of prior and existing research.
- All sources used are properly disclosed (correct citation).
- All authors have been personally and actively involved in substantial work leading to the paper, and will take public responsibility for its content.
- No information obtained for experimentation with human subjects was used.
- No information obtained for experimentation with animals was used.

CRediT Author Statement

Juan Moisés Casas-Peña: Cartography; Data collection; Data curation (petrology, geochemistry); Writing; **Juan Alonso Ramírez-Fernández**: Conceptualization; Methodology; Project administration; Data curation (petrology); **Fernando Velasco-Tapia**: Data curation (geochemistry); **Eduardo Alejandro Alemán-Gallardo**: Cartography; Data collection; **Carita Augustsson**: Conceptualization; Data collection; Data curation (geochemistry); **Bodo Weber**: Data curation (U-Pb); **Dirk Frei**: Data curation (U-Pb); **Uwe Jenchen**: Conceptualization; Methodology; Writing-Reviewing & Editing; Project administration; Fundraising.

Declaration of Competing Interest

The authors declare that they have no known competing financial interests or personal relationships which have or could be perceived to have influenced the work reported in this article.

Acknowledgements

Financial support for this work was provided by a Ph.D. fellowship for the first author from the National Council of Science and Technology (CONACYT; CVU: 630722). The first author, a Ph.D. student at the postgraduate program of the Facultad de Ciencias de la Tierra, Universidad Autónoma de Nuevo León (FCT/UANL), wants to thank Sergio Padilla-Ramírez, Centro de Investigación Científica y de Educación Superior de Ensenada B.C, México and Susana Rosas-Montoya and Daniela Tazzo (CICESE) for their help in the preparation and analysis of the geochronological data. Special thanks to L.A. Elizondo-Pacheco, N.Z. Morales-Alemán, and D.C. Rodríguez-Campero y M. Rodríguez-Escamilla (FCT/UANL) for their assistance in the field. The geochemical and geochronological analyses were supported by the PAICyT projects CT-129–09 and CN-940–19, which was granted by the Universidad Autónoma de Nuevo León. Finally, we would like to thank the "Programa De Fortalecimiento a la Excelencia Educativa (PROFEXCE)" and the Universidad Autónoma de Nuevo León for the support of the field work and the completion of this article.

References

[1] J.M. Casas-Peña, J.A. Ramírez-Fernández, F. Velasco-Tapia, E.A. Alemán-Gallardo, C. Augustsson, B. Weber, D. Frei, U. Jenchen, Provenance and tectonic setting of the paleozoic tamatán group, NE Mexico: implications for the closure of the Rheic Ocean, Gondwana Res. 91 (2021) xxx, doi:10.1016/j.gr.2020.12.012.

[2] J.M. Casas-Peña, J.A. Ramírez-Fernández, F. Velasco-Tapia, E.A. Alemán-Gallardo, C. Augustsson, B. Weber, D. Frei, U. Jenchen, Complete Data Set of Petrological, Geochemical (Major, Trace, and Rare Earth Elements), and U–Pb Zircon Analysis From the Tamatán Group, NE Mexico, Mendeley Data, V1. doi:10.17632/wbzzy6hcgj.1.
[3] R.L. Folk, P.B. Andrews, D.W. Lewis, Detrital sedimentary rock classification and nomenclature for use in New Zealand, N. Z. J. Geol. Geophys. 13 (4) (1970) 937–968, doi:10.1080/00288306.1970.10418211.
[4] W.R. Dickinson, L.S. Beard, G.R. Brakenridge, J.L. Erjavec, R.C. Ferguson, K.F. Inman, R.A. Knepp, F.A. Lindberg, R.T. Ryberg, Provenance of North American Phanerozoic sandstones in relation to tectonic setting, GSA Bull. 94 (2) (1983) 222–235.
[5] R.V. Ingersoll, C.A. Suczek, Petrology and provenance of Neogene sand from Nicobar and Bengal fans, DSDP sites 211 and 218, J. Sediment. Res. 49 (4) (1979) 1217–1228.
[6] W.R. Dickinson, C.R. Suczek, Plate tectonics and sandstone composition, AAPG Bull. 63 (12) (1979) 2164–2182.
[7] G.J. Borradaile, in: Statistics of Earth Science Data: Their Distribution in Time, Space and Orientation, Fifth ed., Springer-Verlag Berlin-Heidelberg, Berlin-Heidelberg, 2003, p. 351 p., doi:10.1007/978-3-662-05223-5.
[8] E. Garzanti, Petrographic classification of sand and sandstone, Earth Sci. Rev. 192 (2018) 545–563, doi:10.1016/j.earscirev.2018.12.014.
[9] W.R. Dickinson, Interpreting provenance relations form detrital modes of sandstones, in: G.G. Zuffa (Ed.), Provenance of Arenites, NATO, 1985, pp. 333–361. ASI S. C 148, D. Riedel, Dordrecht.
[10] U. Jenchen, Petrography and geochemistry of the Triassic El Tranquilo Group, Deseado Massif, Patagonia, Argentina: implications for provenance and tectonic setting, J. S. Am. Earth Sci. 88 (2018) 530–550, doi:10.1016/j.jsames.2018.09.007.
[11] F.J. Pettijohn, Chemical composition of sandstones: excluding carbonate and volcanic sands: data of geochemistry, U.S. Geol. Surv. Prof. Pap. 440 (S) (1963) 1–21.
[12] H.W. Nesbitt, G.M. Young, Prediction of some weathering trends of plutonic and volcanic rocks based on thermodynamic and kinetic considerations, Geochim. Cosmochim. Acta 48 (1984) 1523–1534.
[13] C.M. Fedo, H.W. Nesbitt, G.M. Young, Unraveling the effects of potassium metasomatism in sedimentary rocks and Paleosols, with implications for paleoweathering conditions and provenance, Geology 23 (10) (1995) 921–924.
[14] S.M. McLennan, S. Hemming, D.K. McDaniel, G.N. Hanson, Geochemical approaches to sedimentation, provenance, and tectonics, in: J. Johnsson, A. Basu (Eds.): Processes Controlling the Composition of Clastic Sediments, GSA Special Papers 284 (1993) 21–40.
[15] M.R. Bhatia, K.A.W. Crook, Trace element characteristics of graywackes and tectonic setting discrimination of sedimentary basins, Contrib. Mineral. Petrol. 92 (1986) 181–193.
[16] S.R. Taylor, S.M. McLennan, in: The Continental Crust: Its Composition and Evolution, Blackwell Oxford, 1985, p. 190.
[17] J.H. Stewart, R.B. Blodgett, A.J. Boucot, J.L. Carter, R. Lopez, Exotic paleozoic strata of gondwanan provenance near Ciudad Victoria, Tamaulipas, Mexico, in: V.A. Ramos, J.D. Keppie (Eds.): Laurentia-Gondwana Connections Before Pangea, GSA Special Papers 336 (1999) 227–252.
[18] C. Ramírez-Ramírez, in: Pre-Mesozoic Geology of Huizachal-Peregrina Anticlinorium, Ciudad Victoria, Tamaulipas, and Adjacent Parts of Eastern Mexico, The University of Texas at Austin, Austin, TX, 1992, p. 317 p.
[19] K.R. Ludwig, in: User's Manual for Isoplot 4.1: A Geochronological Toolkit for Microsoft Excel, 5, Berkeley Geochronology Center, Berkeley, CA, 2012, p. 75 p.. Spec. Pub..
[20] J.R. Barboza-Gudiño, J.A. Ramírez-Fernández, S.A. Torres-Sánchez, V.A. Valencia, Geocronología de circones detríticos de diferentes localidades del Esquisto Granjeno en el noreste de México, Bol. Soc. Geol. Mex. 63 (2) (2011) 201–216.